INVESTIGATING THE GAS DISPERSION FROM SUBSEA GAS RELEASES IN SHALLOW WATERS

A Thesis

By

MOUSTAFA HUSSEIN ALI HUSSEIN ALI

Submitted to the Office of Graduate and Professional Studies of
Texas A&M University
in partial fulfillment of the requirements for the degree of

MASTER OF SCIENCE

Chair of Committee,	Luc Véchot
Co-Chair of Committee	Konstantinos Kakosimos
Committee Members,	Marcelo Castier
	Eyad Masad
Head of Department,	M. Nazmul Karim

December 2018

Major Subject: Chemical Engineering

Copyright 2018 Moustafa Hussein Ali Hussein Ali

ABSTRACT

Although the repetitive subsea gas releases incidents occurring in the offshore oil and gas industry, the attention is limited to a case-by-case study; leading to quantitative risk assessment approaches that are limited to similar cases. A subsea gas release can result from a range of different causes including drilling operations; failures in flow lines, gas export lines, and subsea equipment. Such releases can have catastrophic impacts on the environment, offshore platforms, and human lives. Natural gas, in general, and in the Middle East, covers a large portion of the world supply and, consequently, this type of incidents could pose a significant risk for the related and nearby facilities, like Hydrogen Sulfide (H_2S). For example, 40% of the natural gas reserves in the world are sour gas fields in which the Middle East holds the highest reserves of sour gas. While many approaches have been proposed for the description of underwater/subsea releases, these are not universal and still include deficiencies concerning plume turbulence, hydrates formation, and high flowrates water bodies. According to Olsen, 2015, experimental data for underwater releases exist but are also limited to small and medium scale (compared to the actual depth and flow rate). In this study, we investigated the available computational methods to model subsea gas releases cases applicable to the ones of the offshore facilities at the State of Qatar. An Eulerian based computational fluid dynamics (CFD) model was configured in order to study representative gas release scenarios. Earlier, the CFD model was validated successfully against experimental data from SINTEF and Statoil. It also demonstrated the required sensitivity for critical parameters such as the centerline distribution of velocities and void-fraction. Finally, the model was applied for conditions specific to Qatar's offshore industry as a representation of shallow water and a sensitivity analysis was conducted against parameters of local interest such as high-flowrates and

H_2S presence. Finally, a discussion on the potential risk level is given concerning fire & explosion and toxicity hazards like H_2S.

DEDICATION

This thesis is dedicated with love to my family whose affection, love, encouragement and prays days and night make me able to get such success and honor,

Along with all hard working and respected professors.

ACKNOWLEDGMENTS

I would like to thank my committee chair and co-chair, Dr. Luc and Dr. Konstantinos, and my committee members, Prof. Marcelo and Dr. Eyad, for their guidance and support throughout the course of this research.

Thanks also go to my friends and colleagues in The Mary Kay O'Connor Process Safety Center at Qatar and the department faculty for making my time at Texas A&M University at Qatar a great experience.

Finally, thanks to my mother, bother and uncle for their encouragement, patience, and love.

CONTRIBUTORS AND FUNDING SOURCES

This work was supported by a dissertation committee consisting of Dr. Luc Vechot, Dr. Konstantinos Kakosimos and Prof. Marcelo Castier of the Department of Chemical Engineering and Dr. Eyad Masad of the Department of Mechanical Engineering. All work conducted for the dissertation was completed by the student independently.

The graduate student was supported by a fellowship from Texas A&M University at Qatar.

TABLE OF CONTENTS

Page

LIST OF FIGURES

Page

LIST OF TABLES

Page

1 INTRODUCTION

In the context of the current increase in worldwide offshore production of shallow sour gas reserves, there is a growing concern associated with the risks posed by the release of natural gas resulting from the rupture of subsea pipelines. Such release could contain toxic and flammable gases that can pose toxic exposure and fire and explosions issues if it reaches the surface of the sea. Therefore, risks associated to them must be properly addressed and controlled as they can have potentially disastrous consequences.

Subsea gas release, i.e., an uncontrolled release of fluids from a wellhead or wellbore after pressure control systems have failed, has been the source of major concern for the offshore oil and gas industry. The quantification of the risks associated to subsea gas releases require the understanding of the governing physics and the significant parameters that effects the subsea dispersion of gas resulting from a gas release - which is associated with a number of complex phenomenon like turbulence, gas dissolution, hydrates formation etc.- to improve the quality of risk assessment. [2].

1.1 Risk Assessment

Subsea gas releases have numerous potential causes that pose a threat to the offshore platform. It can happen during drilling or production from subsea wells, by the loss of barrier control and by corrosion, erosion, and malfunction in valves and process units, e.g. flow lines & risers [3]. The risks associated to them must be properly quantified and controlled as they can have potentially disastrous consequences. In the context of the current increase in worldwide offshore incidents, there is a growing concern associated with the risks posed by the release of sour gas resulting from

the rupture of subsea pipeline. The quantification of the risks associated with underwater releases requires the understanding of the complex behavior of the bubble plume from an underwater gas release. A review organized by the Norwegian Petroleum Safety Authority (PSA) in 2006 concluded that lack of understanding of subsea dispersion and surface flux is a limiting factor in the consequence modeling.

Risk can be defined as "**A measure of human injury, environmental damage, or economic loss in terms of both the incident likelihood and the magnitude of the loss of injury**" [4]. In a subsea gas release, the likelihood of having a release can be determined from the failure rates of valves and pipelines. These data can be found in various databases (ex, OGP risk assessment data directory, European Gas Pipeline Incident Group "EGIG" & United Kingdom Onshore Pipeline Operators Association "UKOPA") [5]. On the other hand, the magnitude of the subsea gas release can be quantified using consequence analysis. That includes different methods (e.g. source, dispersion and consequence modeling). The consequence modeling deals with the quantification of the severity of the consequences resulted from the Loss of Primary Containment (LOPC) (e.g. toxic releases, fire, and explosions) after the failure of the preventive barriers [6]. The consequence analysis of subsea gas releases does not help in the hazard identification and the risk analysis only, but it helps in preparing the emergency response plan which is part of the emergency management and incident investigation, two of the main pillars of Center for Chemical Process Safety (CCPS) Risk Based Process Safety Management pillars.

Figure 1: Risk-based Process Safety Management pillars

1.2 Subsea Releases Safety Records

The attention towards improving the consequence modeling of subsea releases came after the repetitive major incidents that occurred in offshore oil & gas industry which resulted in significant human and economic losses. Three subsea incidents are presented below.

1.2.1 Al Baz (1989) – Nigeria

A blowout resulted while the drilling operation was conducted in Al Baz field. The gas liberated from the blowout ignited, causing the death of the derrick man. Four other crew members died from impact due to injuries and drowning after jumping overboard to escape the fire. The rig subsequently sank into the sea. “It was a shallow gas blowout that the diverter system could not handle, blowing the 12" diverter lines off from the spool under the bag preventer. The rocks and

sand ignited the gas, with the flames under the cantilever deck" said by one of the off shift drillers on board at the time of the accident.

Figure 2: Al-Baz field collapsing

Figure 3: The platform sank into the sea

1.2.2 Jotun A (2004) – North Sea

On 20th of August, 2004, at 11:20 am, there was a pressure drop in the gas export pipeline inlet from the Jotun field. The pressure drop happened as a consequence of 6 inches' breach in the pipeline about 10 km away from the field. The gas flowed into the sea and reached the surface.

The consequences were limited. The investigation identified a barrier failure related to the installation of the gas export system. The incident was handled in a cooperative effort by ExxonMobil, Gassco, and Statoil. The estimated release rate based on process data was 7 Sm^3/s or 44 kg/s.

Figure 4: Jotun A gas field in the North Sea

1.2.3 Barzan field (2016), Doha, Qatar

Qatar has delayed the start-up of its Barzan Gas project because of a leak discovered in a subsea gas pipeline. According to an engineer working in the project, "There was a gas leakage in one of the project's upstream pipelines, the impact of which is still being assessed"[7]. Leaks in gas pipelines can cause damage to the environment and be challenging to fix, especially if the pipeline is underwater and becomes flooded.

Figure 5: Qatar's map

2 LITERATURE REVIEW

Offshore gas platforms produce natural gas from reservoirs. When a subsea release takes place, buoyancy places an important role as the main driving force to the dispersion of the plume. As the flow rate increases, the force resulted from buoyancy increases as well [3]. This chapter will give an insight on the governing physics behind the buoyant bubble plume, plume zones and the parameters affecting the dispersion of the plume. In addition, consideration of hydrates formation and gas dissolution resulting phenomena will be discussed in this study. The resulted bubble plume from the release will be referred to as a dispersed phase. On the other side, the water and the atmospheric air will be referred to as continuous phase.

2.1 Plume Zones

The release of air/natural gas at some depth in a body of water causes the formation of bubble plume. When the release is high enough it gives rise to a large-scale circulation which is called the turbulence. The buoyant bubble plume resulted from a subsea gas release passes through three main zones of interest as the gas moves towards the surface.

2.1.1 The zone of flow establishment

Depending on the velocity of the release the bubble plume can disperse as bubbling jet (non-choked flow) or a gaseous jet (choked flow) known as “zone of the flow establishment”. [2], [3]

[8]. This zone is dominated by the momentum of the released gas, the formation of the gas jet or the bubble jet. The degree of the bubble formation is governed by the high degree of the turbulence.

Figure 6 and Figure 7 below illustrate different bubble plume zones and the terminologies proposed by many researchers [2], [8]–[10].

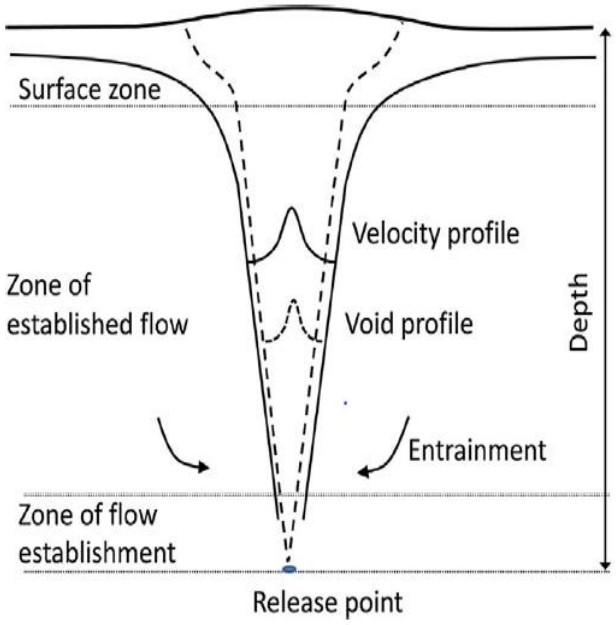

Figure 6: Illustration of different zones and terminology for a subsea gas release "Adapted from [2]"

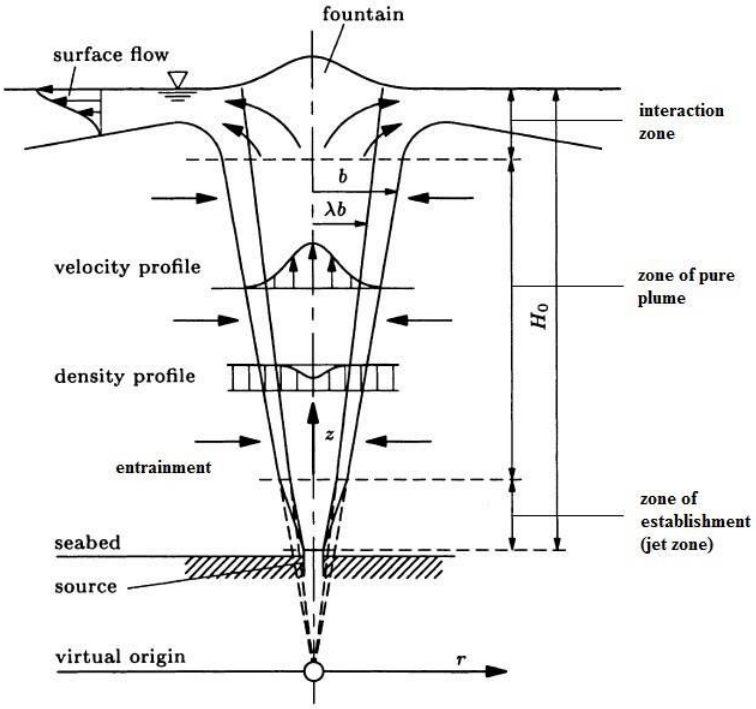

Figure 7: Time-averaged buoyant bubble plume "Adapted from [8]"

2.1.2 The zone of established flow

The jet breaks into a full bubble plume and the gas rises as a dispersed bubble due to buoyancy, where other mechanism appears and are responsible for the movement and spreading of the bubbles, e.g., turbulence and the gas dissolution [2]. The acceleration occurs due to the drag force exerted from the dispersed gas that transfers to water. Due to the drag force effect, the water starts to move with the bubbles formed by creating a motion called *"entrainment of liquid fragments"*[11]. The gathering of the bubbles along the vertical distance forms the bubble plume in the accelerated water which pushes against the water and travels more slowly to the surface. This acceleration is initiated by the first bubbles [3], [8]. The following bubbles experience an additional upwards force due to the water motion generated by the first bubbles. Some of the new bubbles catch up with the first formed bubbles, which cause an accumulation of bubbles in front of the rising plume. This accumulation is known as a bubble cap. The result of the movement of the water column reduces the momentum few meters from the release source point [8], [12].

2.1.3 The surface zone

As the gas covers the water surface, it is released into the atmosphere [2]. The entrained water, unlike the released gas, cannot escape to the atmosphere, however, it disperses on the horizontal surface dragging some of the released gas away from the bubble plume [11]. The gas continues to escape to the atmosphere creating a "boil zone" which is a surface disturbance. In the surface interaction zone referred to in Figure 7, due to the entrained water momentum, the water elevates up in the vertical direction, which refers to as "fountain" [8].

2.2 Effect of the Release Depth

The release depth of the gas is one of the main parameters that is needed to be considered while analyzing the bubble plume. According to Innomar [13], the sea water depth is classified as either shallow or deep. Shallow depth falls between the ranges of 25 to 350 m [14]. The main interest of the project is to focus on releases in shallow stratified waters (ex, Arabian Gulf). Apparently, the maximum depth of the Arabian Gulf is 90 m with an average depth of 50 m [15]. The range of 50 – 90 m falls always in the shallow water range specified by Innomar.

The classification of shallow/deep depth of seawater arises due to the change in the formed bubble plume properties like gas volume, density and the ideality of the gas behavior and the resulted phenomena like hydrates formation, stratification and gas dissolution when the subsea gas dispersion takes place [2].

2.2.1 Effect of depth on density and gas volume

Down at the seafloor, pressures are much higher and temperatures much lower than in the upper water column. This is due to an increase in hydrostatic pressure, the force per unit area exerted by a liquid on an object. The deeper the depth, the greater pressure of the water pushing down on the object according to the following equation. [16].

$$\boldsymbol{P = P_{atm} + \rho g h} \qquad \text{Equation 1}$$

Due to the increase in pressure, the density will change as it varies significantly with pressure and thus water depth has a great effect on the density of the gas in case of both shallow and deep depths

[17]. The physical representation of the pressure-dependent density is applied to the gas expansion as it rises to the surface. The volume of the gas doubles in the last 10 m below the sea surface. As indicated in Figure 8, the gas will be strongly compressed as it goes deeper in the sea. [2], [17].

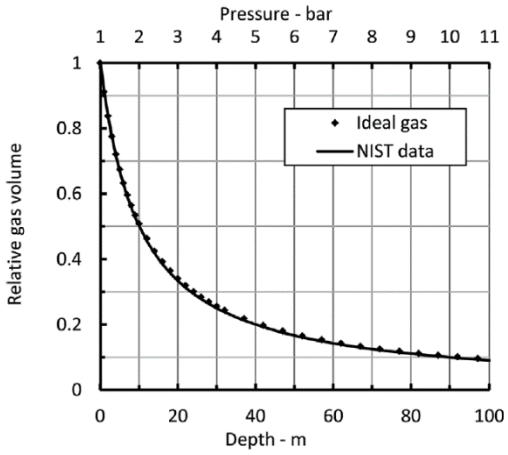

Figure 8: Plot of relative gas volume due to gas expansion as a function of depth "Adapted from [2]"

2.2.2 Effect of depth on the ideal gas behavior

Another significant implication that must be considered in this study is the way the gas is treated either as an ideal or real gas. According to [2], [17], [18], the greater the depth the less accurate the consideration of ideal gas behavior. The bigger the depth, the greater the pressure that will affect the equation of state used. However, as indicated in Figure 9 the relative errors resulted when using the ideal gas law for methane a depth of 500-750 m (Norwegian Sea depth) is approximately 15%, thus, the ideal gas cannot be used in this case.

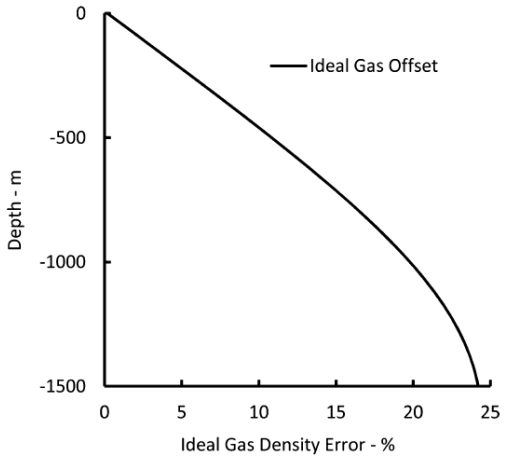

Figure 9: the Relative difference between ideal gas law and the true equation of state for methane "Adapted from [2]"

However, in case of shallow waters, the error is negligible. For example, considering the maximum depth of the Arabian Gulf of 90 m, the error associated is approximately 1.5% and it will be further lower while considering the average depth of 50 m. Thus, in the Arabian Gulf shallow water case, the ideal gas behavior can be used. Various integral models were developed for shallow depth based on this assumption and they showed a good agreement with experimental data [2], [13], [18], [19].

2.2.3 Hydrates formation

Hydrates formation is a serious issue that may occur during the subsea gas dispersion. Subsea releases of gas may enter the water at many different conditions that might be sufficient for

hydrates formation based on many parameters like the rise of temperature, a decrease of pressure or subsea release at high depths [20] [21]. Figure 10 shows the implications of hydrates formation in a subsea gas leak.

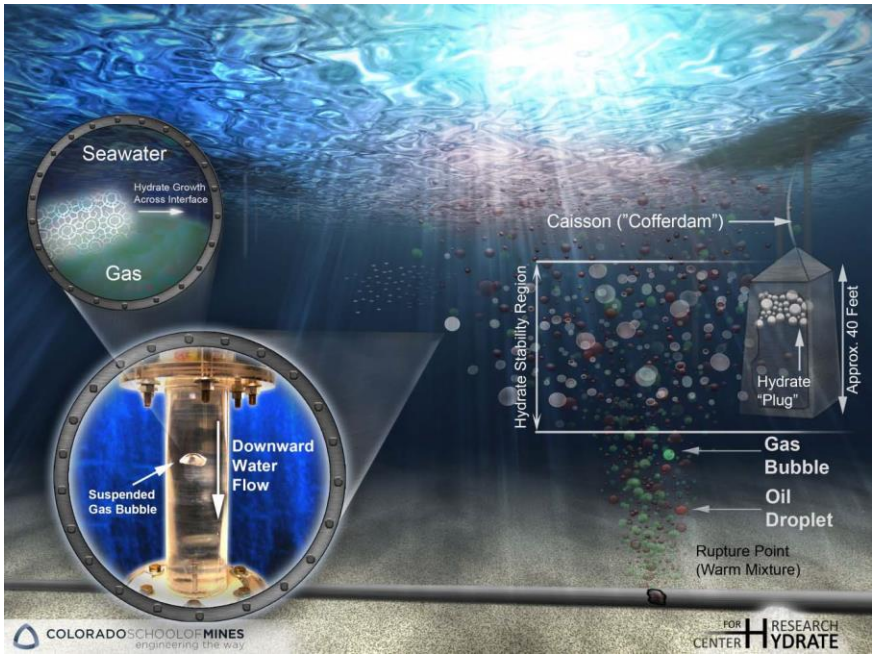

Figure 10: Hydrates formation in subsea gas/oil release "Adapted from [20]"

According to a study done by U.S Department of Energy in the National Energy Technology Laboratory (NETL), when a subsea gas release takes place, the possibility of hydrates formation passes through five different phases/zones as indicated in Figure 11.[20]

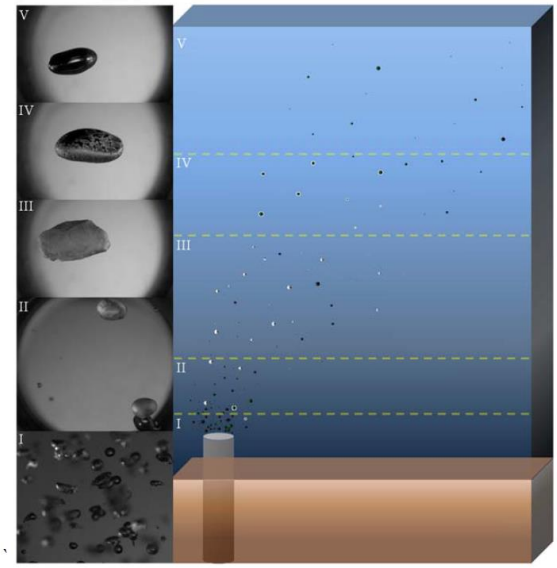

Figure 11: 5 phases/zones for the possibility of hydrates formation in subsea gas releases "Adapted from [20]".

In phase 1, which is referred to as the dense phase, the possibility of hydrates formation to happen in this zone is high due to the elevated gas concentration and to the low temperature of the cold deep ocean [20].

Phase II: the dispersion of the gas will start with minimal bubbles interactions. If the hydrates formation conditions are satisfied, it is likely for the hydrates to form in this zone [20].

Phase III, there will be no bubbles interaction, the bubble plume will start to disperse and the observation of the hydrates is clear [20].

Phase IV and Phase V, the hydrates begin to melt and starts to disappear. The gas will escape to the surface and disperse to the atmosphere. Depending on the water temperature and the released gas pressure/velocity, methane hydrates in subsea releases operations can be found beyond approximately 300 m depth [20], [21].

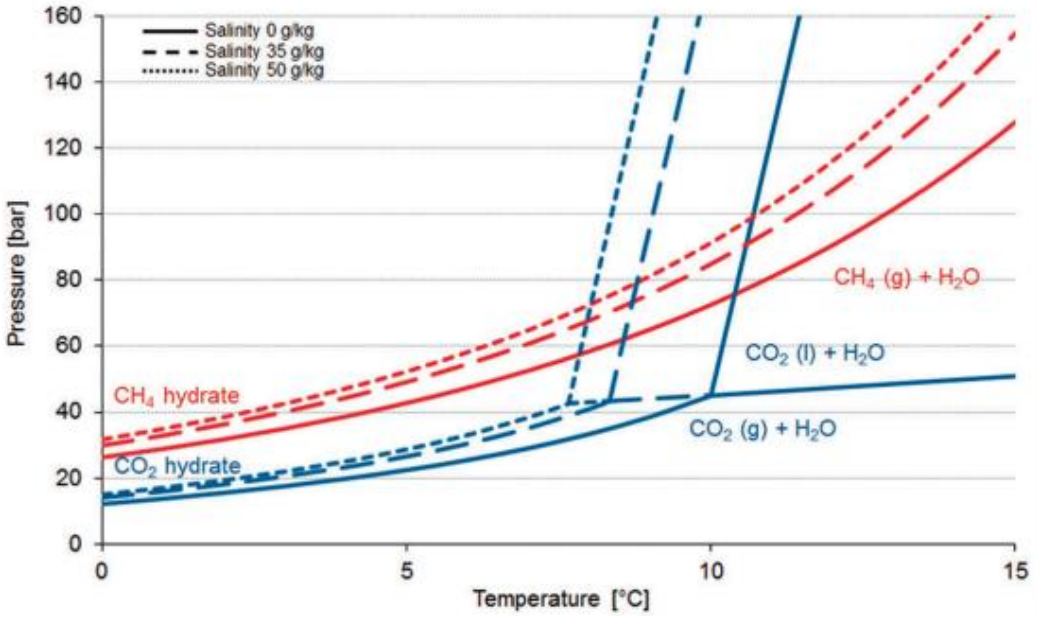

Figure 12: Hydrates stability curves for CO_2 and Methane "Adapted from [21]".

A thermodynamic analysis was done by SINTFF to determine the hydrate equilibrium line for methane in sea water. According to Figure 13, methane hydrates were found to be formed below 600 m depth in the Gulf of Mexico [22].

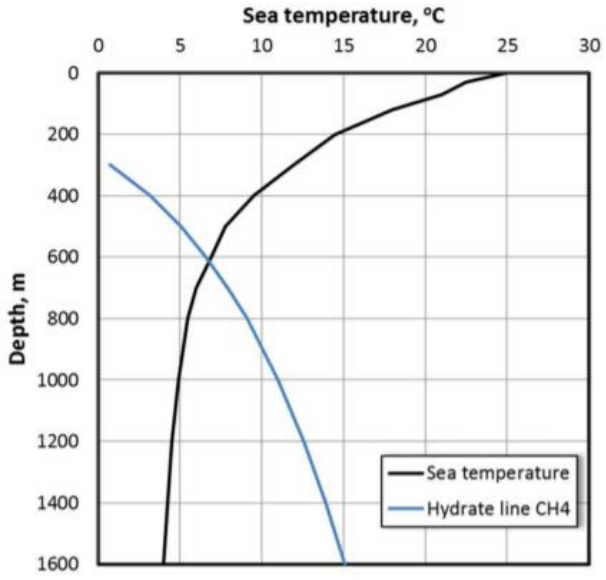

Figure 13: Hydrates formation as a function of depth "Adapted from [22]"

Although the hydrates line is a necessary a sufficient condition for hydrate growth, it can be formed as a thin hydrate shell on the surface of the bubble generated. However, hydrates formation phenomena will not be taken into account in this study as 600 m does not represent the region that the case is built on [18].

2.2.4 Stratification

In multiphase bubble plumes, the gas bubble may get separated from the ongoing plume due to the water stratification. The stratification in this study can be defined as a specific water mass or a specific cross-section volume that has different properties, e.g., temperature, density and salinity compared to different locations in the water body [23]. The water mixing with the bubble plume

can be affected by the layers formed with different water densities due to the stratification effect, as shown in Figure 14.

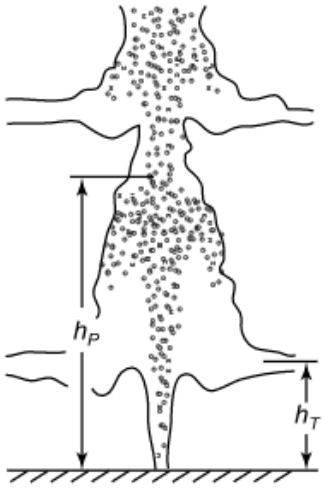

Figure 14: Schematic behavior of oil/gas well subsea release showing pure stratification "Adapted from [23]"

In this study, stratification will not be considered. This thesis assumes constant density, temperature and pure water along the depth.

2.2.5 Gas Dissolution

Dissolution is a mass transfer mechanism driven by the difference of solubility concentrations of gas components and concentrations of already-dissolved gas in the surrounding water. It can be described by the following equation.

$$\dot{m}_i = -\pi d_b^2 k_i (c_i^{sol} - c_i^l)$$ Equation 2

Where, $\dot{m}_i$ refers to the mass transfer rate of gas component i, d_b is the bubble diameter, k_i is the mass transfer coefficient, c_i^{sol} is the solubility and c_i^l is the concentration in the surrounding liquid (water) [2] [3]

In deep water releases, the driving force of the bubble plume –buoyancy- can be vanished due to the dissolution phenomena which is strongly dependent on the sufficient rise time of the bubble plume in the body of water [11]. As the rise time increases, the gas dissolution increases as well. According to the above mentioned equation that is used to calculate the relative gas dissolution by SINTEF and summarized in Table 1 [3], the results show, that at 30 m, and a release rate of 10 kg/s, the gas dissolution percentage was found to be 0.3% compared to almost 100% in 300 m at the same flow rate.

Table 1: The relationship between the gas dissolution and the subsea release depth Reprinted from [3]

	30 m		**300 m**	
	1 kg/s	**10 kg/s**	**10 kg/s**	**100 kg/s**
Rise time (s)	18.7	8.1	502.3	169.3
Mean residence time (s)	18.2	9.6	369.8	170.1
Surface flux (kg/s)	0.93	9.97	0.12	19.2
Relative gas dissolution (%)	6.7	0.3	98.8	80.8
Surface radius (m)	16.9	18.2	69.8	128.5

Thus, it can be concluded that the gas dissolution has negligible effect in shallow water. The gas dissolution effect will not be considered in this study.

2.3 Modeling of subsea gas releases

With the increase in the number of offshore incidents, understanding subsea gas releases is mandatory in the incident investigation – a pillar in the risk-based process safety management CCPS – and since simulating the real cases, especially for high depth is, extremely expensive, computer-based mathematical models became the most effective research tool to understand and to investigate the dispersion of subsea gas releases. Integral models and computational fluid dynamics (CFD) models are two methods used to model subsea gas releases. Integral models use sets of governing equations that are based on an integral over the width of the profiles making the plume models one dimensional with respect to ocean depth. On the other side, CFD models are mathematical models solving the full transient and 3-D Navier-Stokes equations for momentum conservation. CFD techniques are used to solve for the density, velocity, pressure and concentration distribution for the subsea gas releases.

2.3.1 Ditmars and Cederwall (1970)

In 1970, Ditmars and Cederwall developed an integral model to predict the plume width, velocities, and induced flow rates as a function of elevation above the source taking into account the gas compressibility factor. The model assumes the only driving force is the buoyancy and the gas density follows the Boussinesq approximation. The rate of entrainment at the edge of the plume is proportional to the velocity at that height. However, the model was not able to describe the horizontal spreading of the plume and the behavior of the plume near and at the surface. In addition, the study was able to describe the area below the influence of the horizontal flow only.

The model was validated against an experimental study –an air bubble plume study- done by Kobus for small depths of 2 m and 4.5 m. The experimental observation of bubble plume distribution and the integral model did not provide any information on the surface effect. Yet, the model was clearly developed for describing a simple plume driven by buoyancy only. [24] [19]

2.3.2 Fannelop & Sejon (1980)

In 1980, Fannelop and Sejon developed an integral model that describes the gas expansion along with the decrease of the hydrostatic pressure. The model studied the influence of variable buoyancy on the other plume parameters. In addition, it modeled the interaction on the free surface resulting in a radial surface layer. The model assumes the mass flow of the gas is constant along the vertical depth and the density change is described by the variation along the vertical distance by a polytropic relation below of form

$$\frac{\rho_g(z)}{\rho_{g_o}} = \left(\frac{p(z)}{p_o}\right)^{\frac{1}{n}} \qquad \text{Equation 3}$$

The radial distribution of both velocity and density was assumed to have a Gaussian behavior according to the following equation.

$$\bar{\boldsymbol{w}}_{\boldsymbol{p}}(\boldsymbol{r},\boldsymbol{z}) = \boldsymbol{w}_{\boldsymbol{p}}(\boldsymbol{z})\boldsymbol{e}^{-(\frac{\boldsymbol{r}^{\boldsymbol{2}}}{\boldsymbol{b}_{\boldsymbol{p}}^{\boldsymbol{2}}})} \qquad \text{Equation 4}$$

Where $\bar{w}$ is water density, r is the radial distance from the plume mid-point, z is the vertical distance from the point source of the release and b is the buoyancy profile width. The model in addition added an equation for the behavior and the interaction of the gas on the water surface as follows

$$\boldsymbol{\rho_w - \overline{\rho}_p(r,z) = \left[\rho_w - \rho_p(z)\right] e^{-\frac{r^2}{(\lambda b_p)^2}}}$$ Equation 5

Where λ refers to the ratio between the buoyancy and the momentum profiles [9], [10].

The governing equations for the mass and momentum for the bubble plume can be expressed as,

$$\boldsymbol{\frac{d}{dz}\left(w_p b_p^2\right) = 2\alpha_p w_p b_p}$$ Equation 6

and

$$\frac{d}{dz}\left(w_p^2 b_p^2\right) = j\ \frac{\emptyset(z)}{w}$$ Equation 7

where, $j = \lambda^2$ & $w = (\rho_0 - \rho)$ in case of the tophat profile Equation 8

and

$$\boldsymbol{j = 2(1+\lambda^2)\ \ and\ \ w(r,z) = w_m(z) exp\ (-\frac{r^2}{b^2})}$$ in case of the Gaussian profile Equation 9

The model performance was satisfactory up to 10 meters in depth, however, this model failed to describe the dispersion of subsea gas releases from longer depths and high flow rates. Yet, both authors concluded that the further experimental work is required for the better assessment of the applicability of the model. [9]

The authors concluded that the developed equations had described both zone of the flow establishment and the zone of the established flow. However, the accuracy of the equations developed for the surface zone is very poor. The difficulty arises because of the unpredicted turbulence of the bubble plume resulted from the interaction on the surface [9].

2.3.3 Milgram (1983 & 1984)

Milgram proposed an integral model that describes the rise of the bubble plume including the interaction of the gas in the surface zone. The authors used Kobus experimental data [25] to validate the proposed model. The authors assumed that the model follows the isothermal gas law. The liquid depth and the gas density was described as follows [26]:

$$\boldsymbol{\rho_g(z) = \frac{\rho_T(H_B - z)}{H_T}} \quad \text{Equation 10}$$

where, ρ_T is the atmospheric density of the gas. H_T is the atmospheric pressure head. And H_B can be described by the following equation

$$H_B = H_T + H \quad \text{Equation 11}$$

The local mean gas fraction was expressed as,

$$\boldsymbol{f(r,z) = \frac{\rho_w - \rho_p(r,z)}{\rho_w - \rho_g(z)}} \quad \text{Equation 12}$$

The gas volume flux, the momentum flux, and the buoyancy equation were expressed as the following respectively:

$$\boldsymbol{q(z) = 2\,\pi\ \int_0^\infty [u(r,z) + u_b]\, f(r,z)\, r\, dr} \quad \text{Equation 13}$$

$$\boldsymbol{M(z) - 2\pi\gamma\ \int_0^\infty \{u^2(r,z)\rho_w[1 - f(r,z) + [u(r,z) + u_b]^2\, \rho_g(z) f(r,z)]\} r\, dr} \quad \text{Equation 14}$$

$$\boldsymbol{B(z) = 2\pi g\ \int_0^\infty \left[\rho_w - \rho_g(z)\right] f(r,z) r\, dr} \quad \text{Equation 15}$$

Where, u_b is the constant slip velocity and γ is the momentum amplification factor.

Finally, the entrainment hypothesis was proposed by the following equation,

$$\boldsymbol{\frac{dQ}{dz} = 2\pi\alpha\, b(z)\, U(z)} \quad \text{Equation 16}$$

The model assumes a Gaussian profile for the velocity and the density behavior. The model was validated against an experimental data done by Kobus [25]. The experiment was conducted by releasing air at 0.59 Nm^3/s in a 50 m in the United States Naval Research Laboratory. The model concluded that the Gaussian radial profile proposed was limited only to the zone of the flow establishment and the zone of the established flow [26], [27].

2.3.4 Fannelop & Bettelini (1993)

Fannelop and Bettelini [10] used Fannelop & Sejon's governing equations [9] for the mass and a different momentum balance equation. The differences in the models came from the way they assume the behavior of the bubble plume, the boundary conditions and the assumption of some coefficients [10].

It was applied by introducing a shape coefficient φ_i for different shapes of plume behavior according to the following integral governing equations.

$$\frac{d}{dz}\left(\boldsymbol{\varphi_1 w_p b_p^2}\right) = \boldsymbol{2\alpha_p w_p b_p} \qquad \text{Equation 17}$$

and

$$\frac{d}{dz}\left(\boldsymbol{\varphi_2 w_p^2 b_p^2}\right) = \boldsymbol{\varphi_3 g}\ \frac{\boldsymbol{\rho_w - \rho_b}}{\boldsymbol{\rho_w}}\boldsymbol{b_p^2} \qquad \text{Equation 18}$$

where α_p is the entrainment coefficient. The proposed φ_i coefficients were given for both top-hat and Gaussian behaviors in Figure 15 [10].

Coefficient	Definition	Top-hat	Gauss
ϕ_1	$\frac{2}{w_p b_p^2}\int_0^\infty \bar{w}_p r\,dr$	1	1
ϕ_2	$\frac{2}{w_p^2 b_p^2}\int_0^\infty \bar{w}_p^2 r\,dr$	1	1/2
ϕ_3	$\frac{2}{(\rho_w-\rho_p) b_p^2}\int_0^\infty (\rho_w-\bar{\rho}_p) r\,dr$	λ^2	λ^2
ϕ_4	$\phi_3 \frac{w_p(\rho_w-\rho_p) b_p^2}{2\int_0^\infty \bar{w}_p(\rho_w-\bar{\rho}_p) r\,dr}$	1	$1+\lambda^2$

Figure 15: Shape coefficient for plume behavior Adapted from [10]

The mass conservation of the gas can be expressed then as follows,

$$\dot{m}_g = \varphi_3 \pi \rho_g b_p^2 \frac{\rho_w-\rho_p}{\rho_w}\left(\frac{w_p}{\varphi_4}+w_s\right) \qquad \text{Equation 19}$$

The model results show a sensitive behavior with varying the entrainment coefficient. On the other hand, a variation of other parameters had a minor influence on the solution.

Although the model gave an acceptable representation for the behavior of the bubble plume till the zone of the established flow (Figure 6), the model was not able to model the surface zone or to describe the interaction on the surface [9], [10].

2.4 Summary

The research on developing general models to describe the depression of the subsea gas releases has been going throughout the last 60 years. Many researchers developed integral models to predict the dispersion of the gas in a subsea gas release. However, all of these models were limited to modeling the vertical plume and not describing the horizontal dispersion of the gas accurately. In addition, the models did not include the interaction and the dispersion of the gas at the surface or the effect of sea current on the expansion of the gas. The models focused on understanding the governing physics of the subsea gas releases and understanding the parameters and the relationship between the plume properties and the resulting phenomenon occurring (e.g. entrainment and turbulence).

The integral mathematical approach to develop the above-mentioned models were Eulerian integral formulation [28] where the control volume is fixed in space. With the vast amount of work performed and presented in this field, there are some resulted phenomena which required better understanding e.g. turbulence, horizontal dispersion, and surface interactions. Computation Fluid Dynamics (CFD) is more reliable, fundamental, more flexible and possible tool to provide more information on the multiphase dispersion of the gas, formation of the plume and the surface interaction in the subsea environment [2].

2.5 CFD Models

In the last 2 decades, with the increase of the computational powers, Computational Fluid Dynamics (CFD) techniques and tools have been utilized to model subsea gas releases focusing on modeling the surface zone and interactions of the gas on the surface. CFD techniques are now used to solve for the density, velocity, pressure and concentration distribution for the subsea gas releases. ANSYS Fluent 18.1 will be utilized in this study to propose and develop a general model for subsea gas releases in shallow waters.

2.5.1 Moros & Dand (1990)

Moros and Dand model was the first approach to model subsea gas releases using Computation Fluid Dynamics techniques. The software used was PHEONICS a commercial CFD software. The main objective of the model was to provide an assessment of the capabilities of computational fluid dynamics techniques to model subsea gas releases. The turbulence model used was the $k-\varepsilon$ model. The turbulence model for the liquid phase was the standard eddy viscosity model represented by the following equation.

$$\boldsymbol{\nu_t = C_\mu \frac{k^2}{\epsilon}}$$ Equation 20

The effect of the bubble drag force was included in the momentum equation as an external body force. Calculations were carried for a release rate of 10 Nm^3/s in 30 m depth. The model was not validated against any experimental data or mathematical developed models [29].

2.5.2 Swan & Moros (1993)

Fluent was used to predict the behavior of the bubble plume resulted from a subsea gas release. Swan and Moros constructed a model using another commercial CFD software –Fluent-. Gas and liquid phase dynamics were treated separately. The turbulence model used was the $k-\varepsilon$ model. However, a modification was added to the turbulence model, by including a term to account for the turbulence generation by the bubbles. The gas was treated as it consisted of discrete bubbles. A mean bubble size was assumed to be 25 % of the maximum bubble size as calculated by following equation [13] [30].

$$\boldsymbol{d_{max} = 0.35 \left(\frac{q^2 z}{g}\right)^{0.2}} \quad \text{Equation 21}$$

Where q(z) is the gas flow rate and g is the acceleration due to gravity.

The Lagrangian motion was assumed for the bubbles generated using the following equation

$$\rho_g(z)\frac{dV_i}{dt} = -\frac{3\mu_i}{4d_0}(V_i - U_i)C_D R_e + \rho_w U_J \frac{\partial U_t}{\partial x_i} - \frac{\rho_w}{2}\left[\frac{dV_I}{dt} - U_j\frac{\partial U_t}{\partial x_j}\right] - \left(\rho_w - \rho_g(z)\right)g_i \quad \text{Equation 22}$$

Where,

V_i: instantaneous bubble velocity vector

U_i: instantaneous fluid velocity vector

x: coordinate vector

$\rho_g(z)$: gas density

ρ_w liquid density

C_D: bubble drag coefficient

d_p: bubble diameter

R_e: bubble Reynolds number

μ_i: liquid molecular viscosity

The turbulence kinetic energy was expressed as:

$$\boldsymbol{P_b = \frac{q(z)}{N\,\Delta V} \sum_{n=1}^{N} F_t(V_t - U_t)dt} \qquad \text{Equation 23}$$

Where,

P: total turbulence kinetic energy generated

ΔV: cell volume

t: residence time

F: drag force experienced by each bubble

The model was compared against integral models and was able to predict the gas concentration and velocity distribution. However, the model needs more modifications in modeling turbulence and to improve the discretization scheme (mesh sizing) [13] [30].

With the increase of computational powers and the knowledge in CFD, engineers started to develop models for oil and gas releases. The attention came to include both gas and oil because of the increase in offshore incidents resulting in a subsea oil and gas releases [13]. Models developed for both oil and gas release are DeepBlow (2000), CDOG (oil spills) in 2004. However, in 2009, SINTEF Energy developed a general model for subsea gas releases, focused only on the gas releases. The team is developing the model till today.

2.5.3 Cloete & Olsen (2009-now)

The model proposed to use a combination of Discrete Phase Model (DPM) – an Eulerian-Lagrangian- that is used tracking of bubbles motion – with and Eulerian – Eulerian Model Volume of Fluid (VOF) that model that is used to model the sharp interfaces between different phases.

The model solves the Navier Stokes equation for conservation of mass and momentum. The coupled CFD models equations are described below. The mixture density is given by

$$\boldsymbol{\rho = \sum \alpha_q \rho_q} \qquad \text{Equation 24}$$

The viscosity is the sum of the turbulent viscosity and the molecular mixture viscosity

$$\boldsymbol{\mu = \mu_T + \mu_M} \qquad \text{Equation 25}$$

The standard $k - \epsilon$ model is used to model the turbulence. The DPM tracks the discrete bubbles by implementing a force balance on each particle

$$\boldsymbol{\frac{du_p}{dt} = F_D(u - u_p) + \frac{g(\rho_p - \rho)}{\rho_p} + F_p} \qquad \text{Equation 26}$$

The model was validated against the experiment done by Engebrsten et al [1] in Statoil by SINTEF. The model showed an excellent agreement with the experimental data. However, it showed deficiencies in predicting the dispersion of the high flowrate releases.

The authors suggested using the RNG $k - \varepsilon$ turbulence model. This model has a better prediction of void fractions / volume fractions profiles. Cloete and Olsen concluded the wrong predictions of the subsea gas releases model near the surface was due to using standard $k - \varepsilon$ turbulence model and it should be changed in later investigations.

2.5.4 Others

In 2010, a model was developed by Yapa et al [31] focused on deep releases. The model was focused more on the behavior of the bubble plume in the formation of the hydrates formation. As the hydrates formation will not be taken into account in this study, the model will not be further discussed in the literature review section.

3 MULTIPHASE & TURBULENCE

3.1 Multiphase

A multiphase flow can be defined as a flow of the mixture of more than one phase. A phase is a physical state of matter such as solid, liquid or gas. In the context of the project, the multiphase flow will be a mixture of released gas into the surrounded water body (liquid). In the simulation of multiphase flow, the released gas can be referred to as a dispersed phase. On the other side, the water and the atmospheric air will be referred to as continuous phase. In ANSYS Fluent the dispersed phase can be treated as a set of discrete particles (bubbles) in a method called Lagrangian [32].

In Eulerian-Eulerian approach, the phases are considered as an inter-penetrating continua which means that the volume fractions are functions of time and space where the sum of the volume fractions is equal to one [33]. Navier-Stokes equations are derived for each phase in the controlled volume designed. The volume averaged Eulerian multiphase method will be assumed in this study as it accounts for the sharp interface of the gas-liquid interactions on the surface. [34].

3.2 Turbulence

Fluid motion is referred to as turbulent if it is rotational, intermittent, highly disordered and dissipative. Turbulence is a three dimensional, time-dependent, nonlinear phenomena [35].

Turbulence occurs when the Reynolds number $\left(Re = \frac{\rho dv}{\mu}\right)$ of flowing fluid ranges from 2000 to 10^5 [36]. Eddies are the visualization of the turbulence phenomena in turbulent flows Turbulence can be considered to consist of eddies at different sizes as can be seen in Figure 16 [37]. The parallel black lines represent the streamlines in which they are parallel to the mean flow and represent the laminar flow. However, in turbulent flow, eddies of many sizes are superimposed onto the mean flow fluctuations that are formed in all directions.

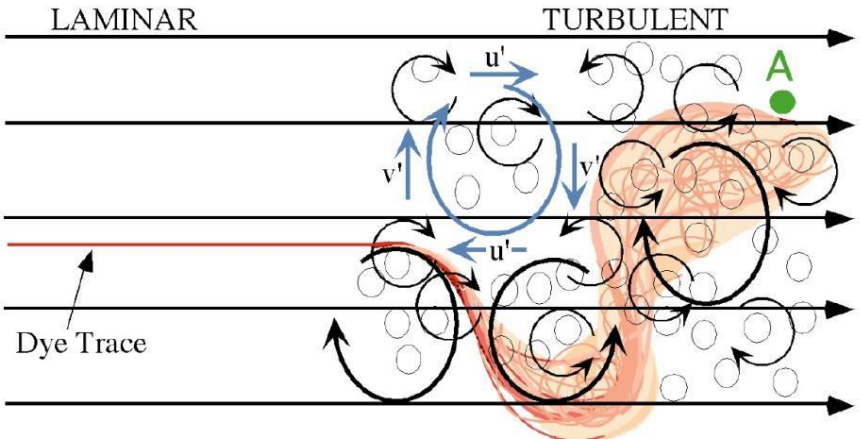

Figure 16: Laminar and Turbulent Flows.

3.3 Modeling Turbulence

The motion of three-dimensional phenomena is described by Navier-Stokes equations. Many models and methods have been developed to model the turbulence (e.g. Direct Numerical Simulation (DNS), Reynolds-Averaged Navier Stokes (RANS) models, Algebraic Stress Models (ASM), Large Eddy Simulation (LES) and the hybrid RANS/LES) [37].

DNS has made a magnificent contribution in turbulence research as it solves the 3D time-dependent Navier-Stokes equations for the whole system designed without the need of any turbulence models. DNS is the most expensive method to solve a flow problem due to the huge memory and computational speed required to accommodate for the small turbulence effects. In addition, it is not available in ANSYS Fluent [36] [37].

The most widely used approach to model turbulence in multiphase problems is RANS models. RANS models focus on describing the mean flow and the effect of turbulence on the mean flow properties. Prior to the application of numerical methods, the Navier-Stokes equations are time averaged for all the resulted eddies. Extra terms appear in the time-averaged flow equations due to the interaction between various turbulent fluctuations. These extra terms are usually modeled using various methods. The most applicable one for the multiphase subsea gas release is the $k-\varepsilon$ model that added two new equations to the averaged equations. The first equation "k" describes the turbulence kinetic energy and the second equations is the turbulence dissipation "ε" which is the rate at which turbulence kinetic energy is converted into thermal internal energy [32], [36].

Turbulence fluctuations are obtained by the decomposition of 3D time-dependent Navier-Stokes equations into mean and fluctuating components (e.g. velocity) described by the following, [32], [36]

$$\boldsymbol{\phi} = \overline{\boldsymbol{\phi}} + \boldsymbol{\phi}' \qquad \text{Equation 27}$$

where ϕ represents the instantaneous scalar quantity, $\overline{\phi}$ is the time-mean value and $\phi'$is the fluctuating component. In addition, the mean value is represented by the following,

$$\overline{\boldsymbol{\phi}} = \lim_{\mathbf{t}\to\infty} \int_{t}^{t+\Delta t} \boldsymbol{\phi}(\boldsymbol{x},\boldsymbol{t})\boldsymbol{dt} \qquad \boldsymbol{t_1} \ll \boldsymbol{\Delta t} \ll \boldsymbol{t_2}$$ Equation 28

Where t_1 represents the time scale of the rapid fluctuations and t_2 is the time scale of the slow motion (for time-dependent mean values e.g. for non-stationary turbulence) [32], [36].

By applying the abovementioned equations to the Navier-Stokes equations, the Reynold Averaged Navier Stokes equations are formed.

$$\frac{\partial \boldsymbol{\rho}}{\partial \boldsymbol{t}} + \boldsymbol{\nabla} . (\boldsymbol{\rho}\vec{\boldsymbol{v}}) = \mathbf{0}$$ Equation 29

$$\frac{\partial \overline{\boldsymbol{u}_i}}{\partial \boldsymbol{t}} + \frac{\partial}{\partial \boldsymbol{x_j}}\left(\overline{\boldsymbol{u}_i}\,\overline{\boldsymbol{u}_j}\right) = -\frac{\mathbf{1}}{\boldsymbol{\rho}}\frac{\partial \overline{\boldsymbol{p}}}{\partial \boldsymbol{x_i}} + \boldsymbol{\nu}\frac{\partial^2 \overline{\boldsymbol{u}_i}}{\partial \boldsymbol{x_j^2}} - \frac{\partial}{\partial \boldsymbol{x_j}}\left(\overline{\grave{\boldsymbol{u}}_{\boldsymbol{\iota}}\grave{\boldsymbol{u}}_{\boldsymbol{J}}}\right)$$ Equation 30

where $\overline{u_i}$ represents the mean velocity, $\grave{u}_\iota$ is the fluctuating velocity, ν the kinematic viscosity and the $\left(\overline{\grave{u}_\iota \grave{u}_j}\right)$ is the Reynolds-stress tensor represented by τ_{ij}.

The stress tensor reflects the effect of turbulence that needs to be estimated to solve the Reynolds Averaged Navier-Stokes equations. Therefore, additional turbulence models must be provided to solve the abovementioned set of equation [35] [38].

Reynolds stress tensors can be appropriately computed using the Turbulence Viscosity Hypothesis that was developed in 1877 by Boussinesq. It is referred to as "Eddy Viscosity Model" and it can be represented by the following equation [32], [36]

$$\boldsymbol{\tau_{ij}} = \overline{\grave{\boldsymbol{u}}_{\boldsymbol{\iota}}\grave{\boldsymbol{u}}_{\boldsymbol{J}}} = \frac{\mathbf{2}}{\mathbf{3}}\boldsymbol{\kappa}\boldsymbol{\delta_{ij}} - \boldsymbol{\nu_t}\left(\frac{\partial \overline{\boldsymbol{u}_i}}{\partial \boldsymbol{x_j}} + \frac{\partial \overline{\boldsymbol{u}_j}}{\partial \boldsymbol{x_i}}\right)$$ Equation 31

and

$$\boldsymbol{\kappa = \frac{1}{2}(\overline{u_i^2} + \overline{u_j^2} + \overline{u_k^2})}$$ Equation 32

Where $\delta_{ij}(Kronecker\ delta) = 1\ if\ i = j\ and\ \delta_{ij} = 0\ if\ i \neq j$, κ is the turbulence kinetic energy and ν is the turbulence or eddy kinematic viscosity (not constant).

Substituting the last two equations in the equation 30

$$\boldsymbol{\frac{\partial \overline{u}_i}{\partial t} + \frac{\partial}{\partial x_j}\left(\overline{u}_i\,\overline{u}_j\right) = -\frac{1}{\rho}\frac{\partial \overline{p}}{\partial x_i} + \frac{\partial}{\partial x_j}\left(\nu + \nu_t \frac{\partial \overline{u_i}}{\partial x_j}\right)}$$ Equation 33

There are different methods developed to solve for the kinematic viscosity with the corresponding appropriate model to be used according to Figure 17 [36].

No. of extra transport equations	*Name*
Zero	Mixing length model
One	Spalart–Allmaras model
Two	k–ε model
	k–ω model
	Algebraic stress model
Seven	Reynolds stress model

Figure 17: Different models to calculate the kinematic viscosity to solve the Reynolds Averaged Navier Stokes Equations "Adapted from [36]"

According to multiphase CFD models developed by Cloete et. al [39], Yapa et. al [31], Christos et.al [37], Olsen et. al [40] and Wu et. al [41], the Two-equation models are the most suitable method in addition to the mean –flow Navier-Stokes equations to model the subsea gas releases. There are many models under the two-equation models (e.g. $k - \varepsilon$ model and $k - \omega$ model). The first equation deals with the turbulence kinetic energy (k) and the second one with either the

dissipation rate of kinetic energy (ε) or the specific dissipation rate (ω). The choice of the second equation depends relies on the application. In the context of this project, the $k-\varepsilon$ model is suitable for the modeling of multiphase subsea gas releases.

3.3.1 Standard $k-\varepsilon$ model

The $k-\varepsilon$ model is the most widely used and tested among all the models mentioned in Figure 17. The standard $k-\varepsilon$ model of Launder and Sharma [42] is defined as follows:

Kinematic eddy viscosity (ν_t) equation:

$$\boldsymbol{\nu_t = C_\mu \frac{k^2}{\varepsilon}} \qquad \text{Equation 34}$$

Turbulence kinetic energy (k) equation:

$$\boldsymbol{\frac{\partial k}{\partial t} + \overline{u_j}\frac{\partial k}{\partial x_j} = \frac{\partial}{\partial x_j}\left[\frac{(\nu+\nu_t)}{\sigma_t}\frac{\partial k}{\partial x_j}\right] - \varepsilon + \tau_{ij}\frac{\partial \overline{u_i}}{\partial x_j}} \qquad \text{Equation 35}$$

Turbulence dissipation rate (ε) equation:

$$\boldsymbol{\frac{\partial \varepsilon}{\partial t} + \overline{u_j}\frac{\partial \varepsilon}{\partial x_j} = \frac{\partial}{\partial x_j}\left[\frac{(\nu+\nu_t)}{\sigma_\varepsilon}\frac{\partial \varepsilon}{\partial x_j}\right] + C_{\varepsilon 1}\frac{\varepsilon}{k}\tau_{ij}\frac{\partial \overline{u_i}}{\partial x_j} - C_{\varepsilon 2}\frac{\varepsilon^2}{k}} \qquad \text{Equation 36}$$

where σ_t = 1.0 and σ_ε = 1.3 are the Prandtl numbers for k and ε, respectively. The model constants are: C_μ= 0.09, $C_{\varepsilon 1}$ = 1.44, $C_{\varepsilon 2}$ = 1.92.

The model was not able to predict the accurately the flows with huge pressure and high release flowrates gradient and rotational movements which results in poor predictions in high depth / high flowrates multiphase flows [43].

3.3.2 RNG $k-\varepsilon$ model

This model is based on a statistical technique theory proposed by Yakhot and Orszag [44] called the Renormalization Group. The RNG $k-\varepsilon$ model is the modification of the standard $k-\varepsilon$ model. C_μ is no longer constant but it is computed in RNG model by the eddy viscosity equation.

The additional term added to the RNG $k-\varepsilon$ equations improved the accuracy of predicting the rapidly strained flows (high flow rates), the behavior near the near-wall region and the surface interactions [41], [45].

The model is represented by the same kinematic eddy viscosity (ν_t) equation and turbulence kinetic energy (k) equation, however, the modification comes as the following:

$C_{\varepsilon 2}$ *i*s computed by the following equation

$$\boldsymbol{C_{\varepsilon 2} = C_{\varepsilon 2} + \frac{C_\mu \eta^3 \left(1-\frac{\eta}{\eta_0}\right)}{1+\beta_1 \eta^3}} \qquad \text{Equation 37}$$

with $\eta = \frac{Sk}{\varepsilon}$, $S = \sqrt{2S_{ij}S_{ij}}$ and $S = \frac{1}{2}\left(\frac{\partial \overline{u_i}}{\partial x_j} + \frac{\partial \overline{u_j}}{\partial x_i}\right)$

where S indicates the mean strain-rate of flow and S_{ij} is the deformation tensor and the constant of the model are $C_\mu = 0.085, C_{\varepsilon 1} = 1.42\ C_{\varepsilon 2} = 1.68,\quad \sigma_\varepsilon = \sigma_k = 0.72\ , \beta = 0.012\ and$ $\eta_0 = 4.38.$

The RNG $k-\varepsilon$ model will be used to model turbulence in this study due to the discrepancy of the standard $k-\varepsilon$ model in predicting the flow in case of the high flow releases and predicting the

interactions on the surface. The main reason for this discrepancy in that the standard $k-\varepsilon$ does not account for the turbulence damping in the vicinity of a free surface. In addition, the RNG model is more responsive to the effects of rapid flows and account for many parameters that are not modeled by standard model (e.g. swirl effect, local turbulence) in case of the multiphase subsea gas release.

4 THESIS OBJECTIVE

While many approaches have been proposed for the description of underwater/subsea releases, these are not universal and still include deficiencies concerning plume turbulence, modeling high flowrate scenarios and describing the interactions on the free surface. All the above-mentioned deficiencies will influence the Quantitative Risk Assessment. The objective of this research is to investigate the available computational methods and propose the most appropriate model for subsea gas releases and to provide a better understanding of released fluids behavior. The research outcomes will refine the scope of subsea blowout risk management by identifying the consequences of the subsea gas releases on the surroundings in the State of Qatar offshore platforms. Computational Fluid Dynamics (CFD) has the ability to become an important tool in the future advancement of the understanding of the subsea gas. A detailed description of the model will be presented and discussed. The model will be verified against an existing experimental data measured by Engebrsten et al [1] before applying the model to Qatar's offshore platforms conditions and properties. Then the developed model will be applied to investigate subsea gas released in Qatar's offshore platforms. The model, in addition, will be used to provide reliable literature data to the offshore industry to cover the range of concern in depth/rate chart of known subsea gas releases [2], [3].

5 METHODOLOGY

5.1 Selection of the experiment

Any model that predicts a behavior of phenomena has to be validated against a trusted model or experimental data with a specified error criterion. According to Olsen (2015), scientists and engineers are trying to find the most credible model to understand subsea releases with the largest depths and highest flow rates possible. A trusted well-designed experiment is to be selected to validate a designed model [2]. Many experiments had been carried out to understand and model the subsea gas releases according to the table provided below.

Table 2: Literature experiments for subsea gas releases

Experiments	Water Depth (m)	Release Rate (Nm^3/s)
Topham 1956 [46]	23	0.06-0.65
	60	0.30-0.40
Kobus 1968 [25]	4.5 - 5	0.00013-0.0062
Fennelop & Sjoen 1980 [9]	9.9	0.005-0.022
Milgram & Van Houten 1982 [27]	4	0.00021-0.00023
Milgram 1983 [26]	50	0.024-0.95
Loes & Fannelop 1989 [47]	50	0.6 -1.3
SINTEF 1997 [1]	7 m	0.083 - 0.750

From the above-mentioned table, the criteria for selecting an experiment is as follows:

1- The accuracy of the data and information available based on a literature search.
2- High flow rate.
3- Depth.
4- Times used to validate another model.

Applying the above-mentioned criteria and a decision was made to select SINTEF 1997 experiment that was done by Engebrsten et al [1].

Engebrsten et al.‘s [1] experiment was designed by Engebrsten from SINTEF, Northug from Statoil research center Norway, Sjoen from Statoil and Fannelop from ETH. The experiment had been carried out in a 7 m deep basin in Statoil’s research center releasing a mixture of air and helium at different flowrates. The parameters estimated were as follows:

1- Vertical and horizontal plume velocity
2- Void fractions in a vertical plume
3- Vertical and horizontal gas concentration
4- Bubble shape and movements.

The experiment was conducted in pure fresh water with a video recorder at several positions. Air was released when parameters below the water surface were to be investigated. A mixture of 40% He and Air was released when the concentration measurements were to be investigated to simulate the buoyancy of the Natural Gas. The pressure was kept constant by a regulator depending on the desired value of the flow rate. This experiment was chosen as a representative subsea gas releases

case study in this thesis because of the accuracy of the measured parameters [48]. In addition, the experimental data was used to validate the three CFD models [41], [48], [49] and an integral model [10] because of the accuracy of measured data with the variety of the parameters recorded. The results were recorded at the surface and analysis of the gas transport above the bubble plume were carried out. Although the experiment's depth is 7 m only, the experiment is reliable in our case because of the accuracy of measured data with the variety of the parameters recorded. Once the model is validated the depth will be expanded and varied as will be defined in case studies.

5.2 CFD Modeling

Computational Fluid Dynamics (CFD) is a computer-based mathematical tool for understanding and analyzing real flows through numerical simulations of some governing equations [50]. CFD provides cost-effective solutions by solving conservation of mass, momentum, and energy. These equations are used and combined together to form Navier Stokes equations [36]. Navier-Stokes equations are solved using an approximation of the partial differential equations by the set of algebraic equations [51]. In this project, ANSYS Fluent 18.1 will be utilized to solve the Navier-Stokes equations (Appendix A) using a discretization method called "Finite Element Volume" where the governing partial differential equations are converted into algebraic equations with the assigned discrete elements [52]. There are a large number of packages in ANSYS Fluent 18.1 that are employed to solve the multiphase subsea gas release- presented in this work.

The definition of CFD case goes through several stages as follows, [36] [32]

1- Creating the geometry

This is where the geometric model is build using the function in a preprocessor called ANSYS Fluent Design Modeler. The geometry represents the domain of the system which is going to be a 2D framework of 6 m width by 10 m height and a release diameter of 10 cm in the middle. [32], [52].

2- Mesh sizing

In order to solve for the parameters required, the domain must be divided into numerical grid cells. It is also known as a mesh. The process is called mesh sizing and it is done in the preprocessor. ANSYS Fluent provides an adaptive way to do an estimate adaptive mesh sizing and the user can refine the mesh proposed if needed. [52]

3- Model selection and boundary conditions

The mathematical model and the parameters that describes the phenomena are selected once the geometry is set and the mesh sizing is done. The required boundary conditions are defined and tuned for the structured domain so the calculation activity can start. [52]

The specification will be as follows:

1- The simulation will be an unsteady state.

2- Methane will be released into a body of water and there will 3 m of air above the surface of the water.

3- Eulerian three phase will be selected for air, water, and methane.

4- Turbulence model selected will be RNG $k - \varepsilon$ model

Different velocity/flowrates values will be simulated. The release diameter will be varied as well.

4- Calculation Activities

A set of algebraic equations are yielded using the discretization method for each cell. This set of equations is solved using iterative methods with the help of the defined boundary conditions and models selected. Errors, also known as residuals, are computed after each iteration until the residuals become sufficiently small [52].

5- Convergence

When the residual values in the system reached to a small value (10^{-3} to 10^{-4}), the convergence is reached. The residual can be calculated using the following equation,

$$R^{\emptyset} = \frac{\sum_{cell\ P} |\sum_{nb} a_{nb}\emptyset_{nb} + b - a_p\emptyset_p|}{\sum_{cells} P|a_p\emptyset_P|}$$

Where, $\emptyset$ is the variable, $a_{nb}$is the influence coefficients for the neighboring cells and a_p is the center coefficient. Convergence is the indication of the success of the running simulation. In case of a steady-state simulation, the calculation stops once the convergence is reached [36], [52]

6- Post processing

Once the simulation is completed and converged, the solution can be seen for the parameters calculated in graphs, numerical values, contour maps and video animations to be analyzed and discussed [52]. The parameters of interest are:

1- Concentration profile/centerline void fractions or centerline volume fractions of methane in the body of water and air.

2- Rise time: the time it takes the plume from the release point to the water surface.

3- Centerline velocity profiles.

4- Pressure

5- The density of the gas.

5.3 Validation of the designed model

After the results (contour maps and graphs) are generated, the data will be plotted against the experimental data from Engebrsten et al. [1] to be studied and discussed. The graphs and data generated will as follows:

1- Graphs of velocity vs. vertical distance from the source.

2- Centerline Void fraction vs vertical distance from the source.

3- Rise time data for each velocity simulation.

4- Pressure contour maps will be presented.

A comparison will be done between the experimental data and our simulation results. Errors will be calculated and discussed with a certain criterion. A conclusion will be drawn afterward.

5.4 Qatar's Case – expansion of the model

Once the model is validated, it will be expanded to model Qatar's offshore subsea gas releases. Different release flowrates will be simulated for different release diameters.

In addition, part of depth/rate chart of known subsea gas releases proposed by SINTEF will be covered by our simulation ranges [2] as shown in Figure 18.

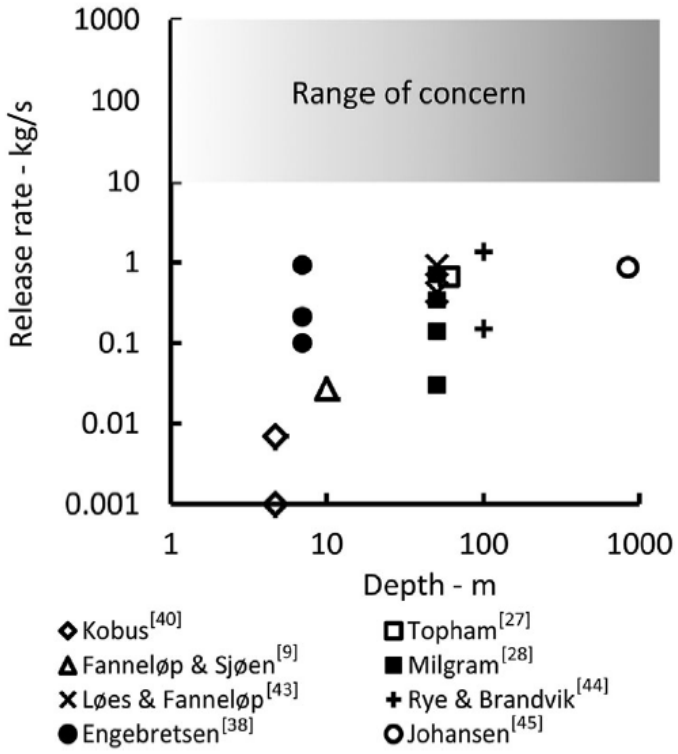

Figure 18: Depth/rate chart of subsea gas releases "Adapted from [2]"

6 IMPLEMENTATION

The main goal of the CFD modeling in this project is to construct a model to model subsea releases. The model should achieve reliable and accurate results. The method illustrated in section 5.2 will be followed to construct a subsea gas release model followed by a validation to assure the reliability of the designed model in predicting subsea gas releases.

6.1 Creating the geometry

The geometry was created in the design modeler in ANSYS Workbench identical to the experimental basin done by Engebrsten et al. [1]. A two-dimensional geometry was designed as follows:

- Water Body Domain size: 6 m x 7 m
- Release point: at 3 m in the x-axis (Center of the domain)
- Release point: 0.1 m diameter

An air body was added on the top of the water with a domain size of 6 m x 3 m. The purpose of the air body is to model surface interactions and to account for the backflow and fountain effects. Figure 19 shows the constructed domain in the design modeler in ANSYS Workbench.

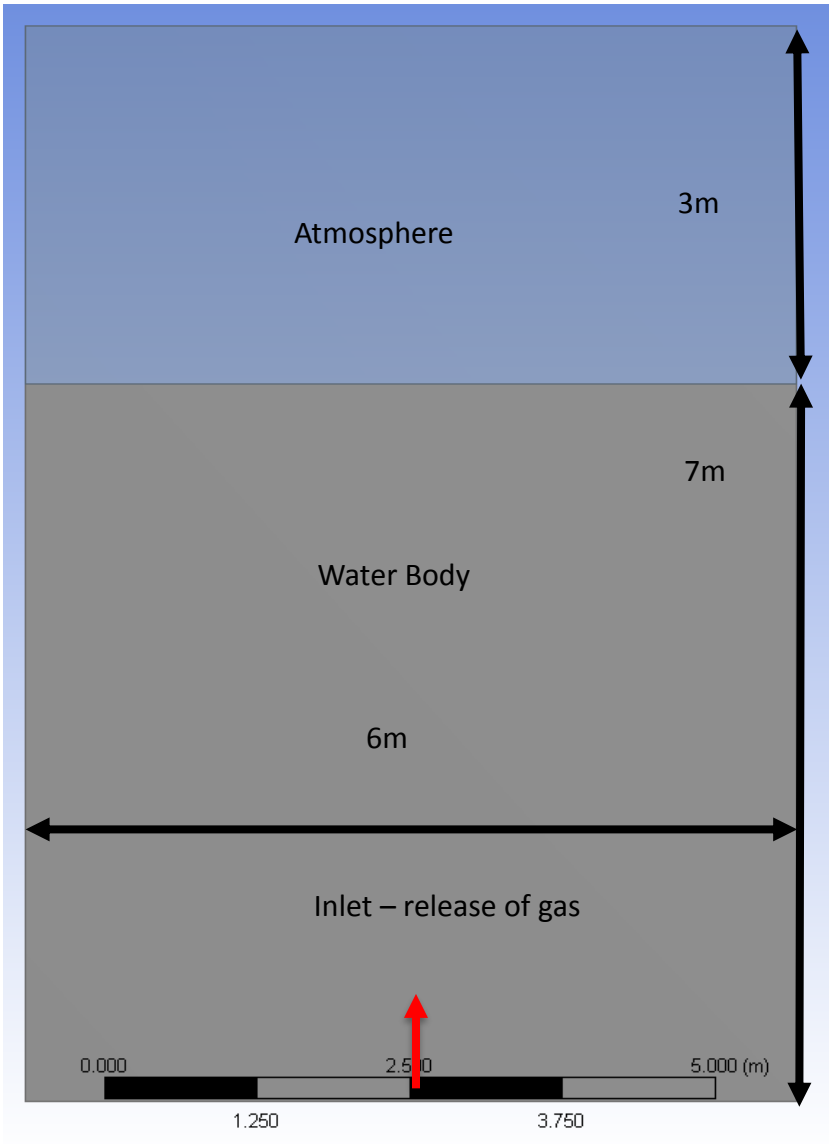

Figure 19: Geometry designed in ANSYS Workbench

6.2 Mesh Sizing

The geometry is to be divided into a uniform grid size distribution to solve for the desired properties. First, the geometry is exported to mesh step in the workbench. An automatic mesh is generated for the abovementioned geometry in Figure 19. The geometry was divided into 1396 hexahedral cells. A mesh refinement step was carried on to improve the grid as it is required for the accuracy of the result. The first stage of the refinement stage can be shown in Figure 20 with 3315 cells with finer grid sizes in the jet zone (release point) as this zone has a large gradient change in the flow variables.

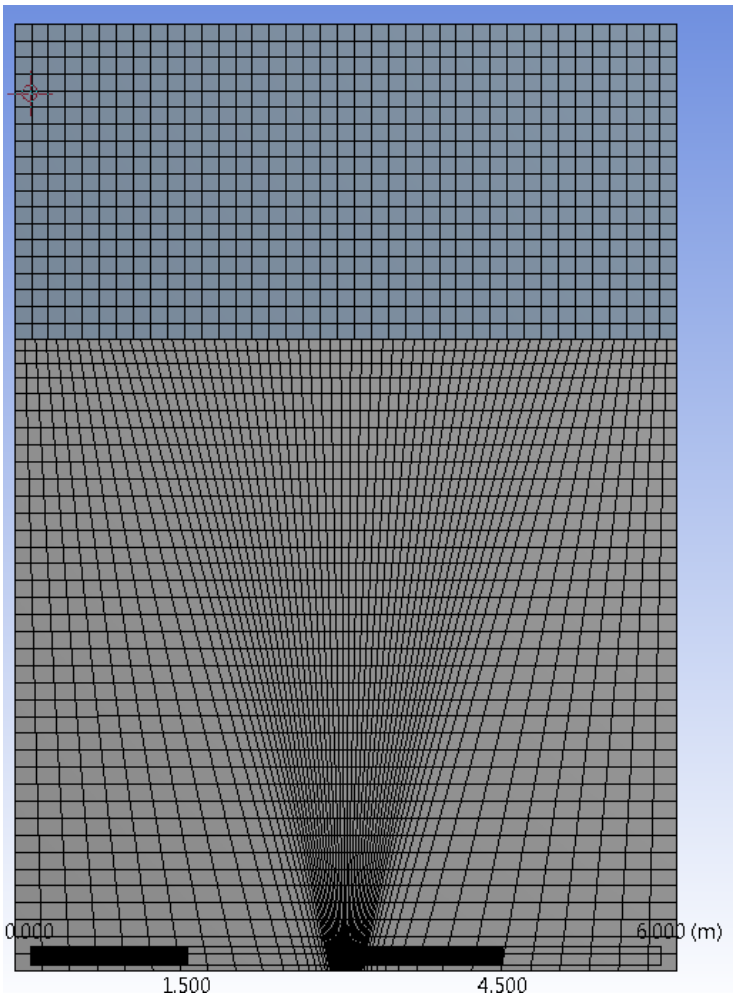

Figure 20: a 1st trail of the grid refinement stage

A second refinement stage was carried out to further improve the grid focusing on the surface to accurately describe the interaction in the surface zone. Growth rate, inflation option, and size function were varied to further improve the grid and achieve the desired mesh. This step was found to be time-consuming due to required preliminary knowledge about the process of the bubble

plume dispersion and the areas with the large gradient change in flow variables. The abovementioned parameters were varied as follows:

- Element size: 1 cm
- Growth rate: 1.2
- Inflation option: Fine
- Size function: proximity and curvature

An edge face meshing was added for the bottom to further improve the nodes in the release point. It divided the release point into 20 divisions with a uniform size function with a growth rate of 1.050. The simulation was performed with 9203 quadrilaterals cells shown in Figure 21.

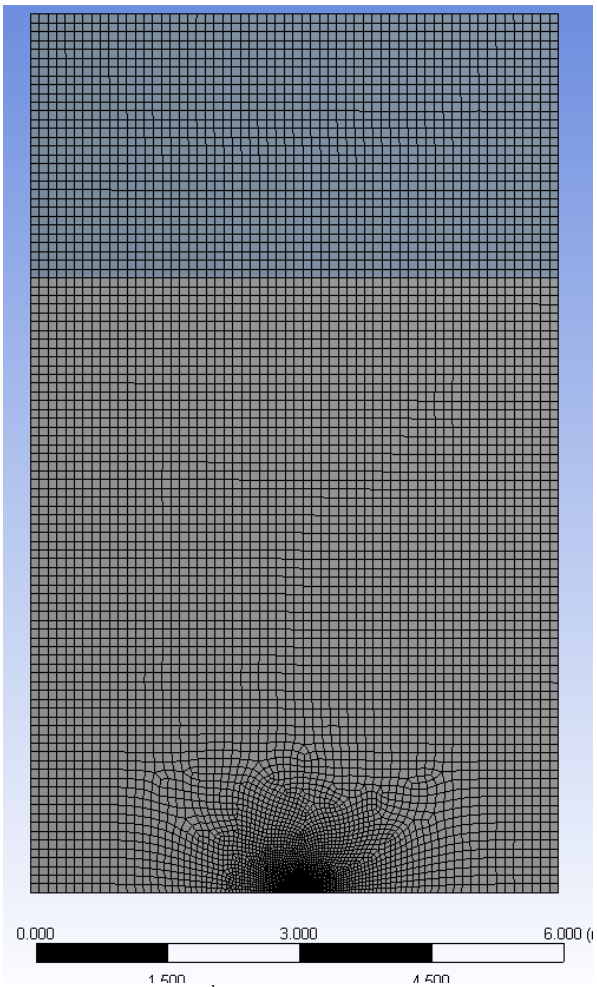

Figure 21: a 2nd trail of the grid refinement stage

A third refinement stage was carried out further improve the grid focusing on the surface to accurately describe the interaction in the surface zone. The following parameters (growth rate, inflation option) were kept as in the second stage but the element size was reduced to be 0.5 cm. The simulation was performed with 26479 quadrilaterals cells shown in Figure 22.

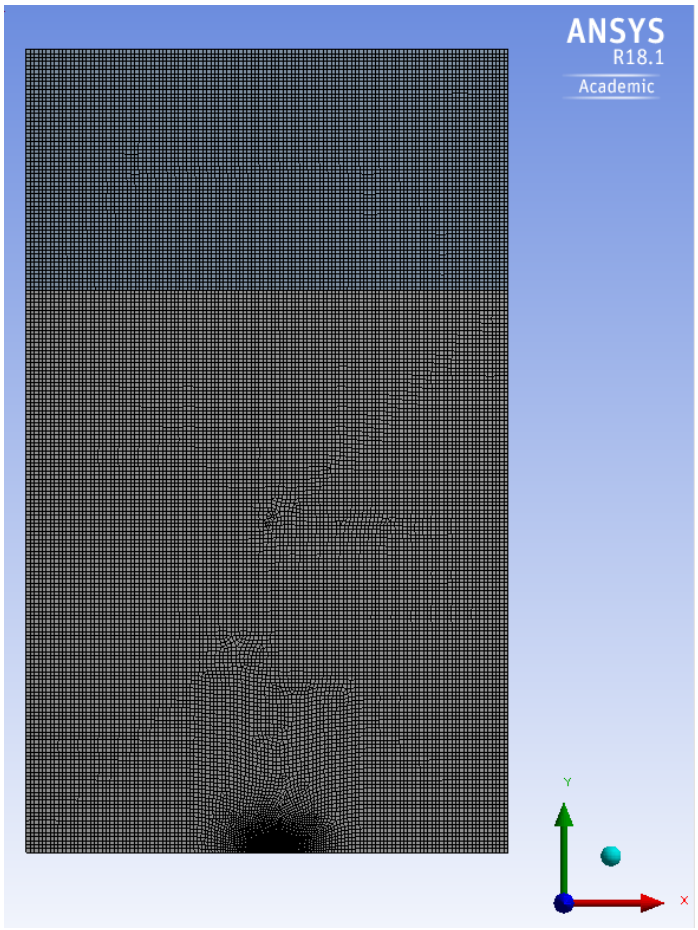

Figure 22: 3rd trail of the grid refinement stage

With the developed three grids, one must be selected to perform the simulations. The solution may differ from a grid to another because of the difference in the mesh resolution. A mesh independence study was conducted on the three designs to assure that the solution is independent of the mesh resolution. The process is as follows:

1- Run an initial simulation for the three cases and ensure convergence of residual error is between $10^{-3}\ to\ 10^{-4}$. If this criteria was not met, the mesh should be refined.

2- Monitor the error resulted for values of interest (e.g., methane velocity at a certain depth) and compare the resulted errors.

3-

If convergence residuals and the velocity errors did not change, the solution is independent of the mesh resolution. The results of the mesh independency study are presented in Table 3.

Table 3: Mesh independency study results

Mesh cells	**5 cm cell size**	**1 cm size with a focus on the release point**	**0.5 cm size with a focus on the release point**
No. of Cells	3315	9203	26879
Simulation Residuals	10^{-1} to 10^{-2}	10^{-3} to 10^{-4}	10^{-3} to 10^{-4}
Methane Velocity Residuals	10^{-3} to 10^{-4}	10^{-6} to 10^{-7}	10^{-6} to 10^{-7}
Approx. Simulation Time	2 hours	8 hours	One Day

The decision was taken to select the second refinement stage. The simulation's residuals and the velocity's residuals fall in the acceptable convergence range. In addition, the computational time is moderate compared to the third refinement stage providing the same residuals' order of magnitude.

6.3 Model Selection and Boundary Conditions

After the model is designed and the mesh is ready, the system setup step is now activated in ANSYS Workbench where materials, models boundary conditions, solution activities and pre-processing activities should be set. As mentioned in chapter 5, the Transient Eulerian-Eulerian model will be selected for the multiphase flow along with the RNG $k-\varepsilon$ model to account for turbulence. In this section, phases were defined to be three for liquid, gas and liquid-gas mixed phase resulted by the dispersion of bubble plume in the water body. Materials were selected to be:

- Air for the air body (atmosphere).
- Water for the water body.
- Methane: the released gas in the water body.

6.3.1 Boundary Conditions

Before running the simulation, the CFD should choose the appropriate Boundary condition to run the simulation. The choice was done based on the experimental conditions defined by Engebrsten et al. [1]. This section will illustrate all the conditions added to the system to be set to run the simulation.

Inlet boundary condition: was set as a velocity inlet activated only for methane. The velocity of released methane was varied according to the experimental release conditions by Engebrsten et al. [1]. The velocity of water and air was assumed to be zero.

Outlet Boundary: was set as pressure outlet at the atmospheric pressure and zero gradients for the other variables. The backflow volume fraction was assumed to be zero for both water and methane.

Interfaces: An interface was created to separate the water body and air body to specify the initial conditions. The specification of the initial conditions is referred to as the "Solution Initialization and Patching".

6.3.2 Solution Initialization and Patching

In this section, the initial conditions are set automatically by the ANSYS Fluent by standard initialization method to run the simulation. Constant values are assigned to the parameters solved to start the simulation. Another step required in the solution initialization section is to patch the section. Patching is specifying different initial conditions to some sections in the designed grid. In this designed grid, the volume fraction of water have been specified to be equal to 1 in the water body. Similarly, in the air body, the volume fraction of air was specified as 1 to define the atmosphere area as shown in Figure 23.

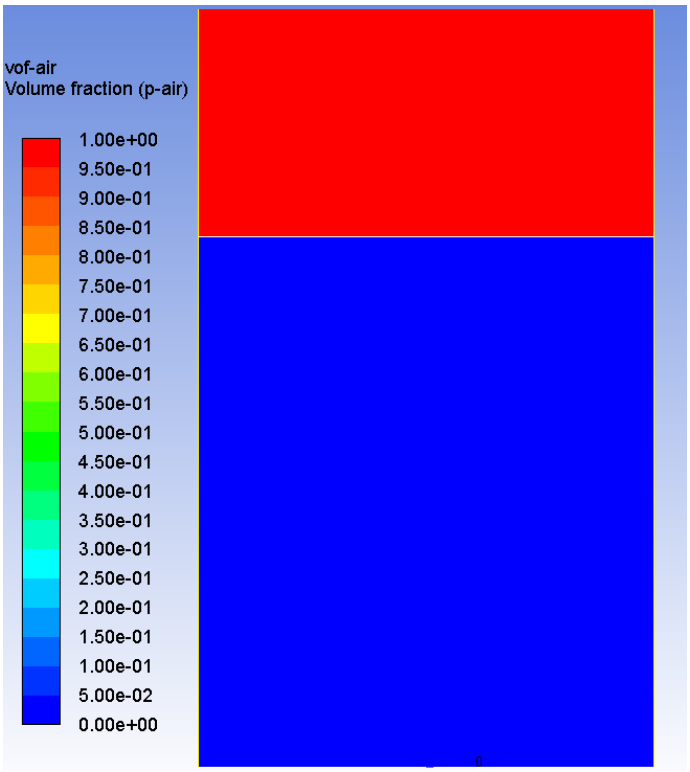

Figure 23: Patching Step to define air and water bodies

6.4 Calculation Activities

The time stepping method selected to run the simulation is adaptive. The adaptive method gives an automatic determination of the time step size that is based on the estimation of the truncation error associated with the time integration scheme. The CFD user specifies a range in ANSYS Fluent to work along with the ending time of the simulation. Figure 24 shows one of the scenarios simulated using the adaptive method. The gas was released for 20 seconds with an adaptive time steps setting allowing time steps to range between two values as indicated below based on the estimation of the truncation error associated with the time integration scheme [32].

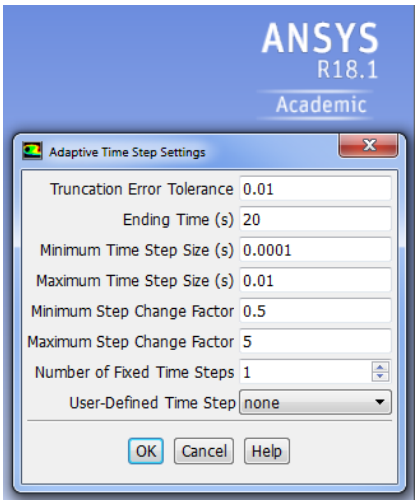

Figure 24: Adaptive time step settings

6.5 Critical Parameters

Some considerations must be taken into account before running the simulations.

6.5.1 Non-release Scenario

A non-release transient scenario was run first before injecting any gas into the body of water. The idea of running the simulation, without methane injection, is to define the water and air properties in both air and water bodies and to assure that the pressure distribution had developed. Figure 25 shows the simulation results of the non-release scenario with the pressure distribution in the water body. As the depth increases, the pressure increases as well. As can be seen at the depth of 7 m, the corresponding pressure is $1.7 \times 10^5\ Pa$.

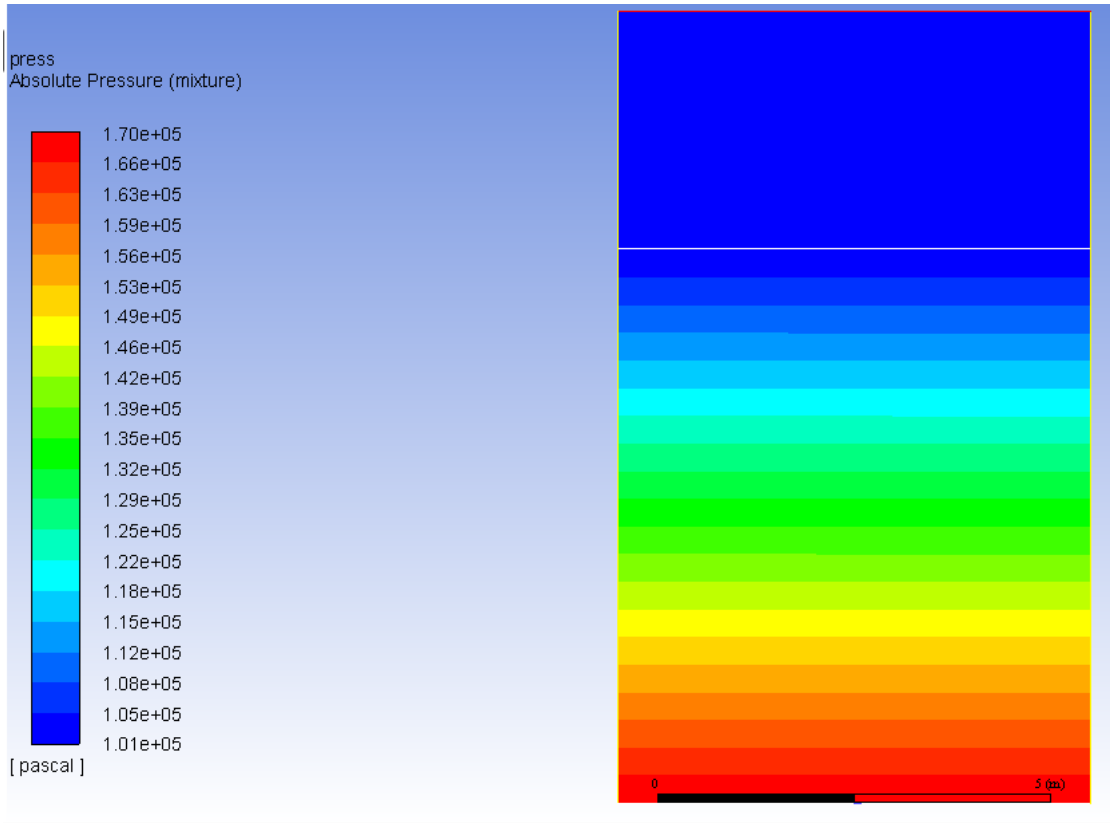

Figure 25: Pressure contour map of the non-release situation

6.5.2 Solution Method,

The continuity, momentum, and turbulence are derived from the Second-Order Upwind and QUICK, which are based on higher-order schemes. The higher the order the more accurate the solution will be and the more computational power and time required to run the simulation [32].

6.5.3 Hardware and Software

The calculations are achieved by submitting the ANSYS Fluent simulation files onto a high-performance cluster referred to as -Supercomputer RAAD 2- at Texas A&M University at Qatar.

7 MODEL VALIDATION

A subsea gas release experiment was conducted in Norway (1997) at Statoil's Research center. The experiment was done by Engebrsten et al. [1] under the name of "Rotvoll". The experimental findings were presented in a paper published in Engebrsten et al. [1].

The purpose of the experiment was to investigate a bubble plume resulted from underwater gas release and the dispersion of the gas near the surface. Series of releases were done in a basin filled with water. The experiment was conducted in a pool of 7m deep and a surface area of 6x9 m.

The gas was released at 3 different rates according toTable 4. A pipeline was connected between the vessel and the point of the release to reduce the vertical momentum created by the bubble plume. In addition, a momentum breaker was installed to minimize the gas flow fluctuation [1]. The only information missing in this paper was the release diameter. To overcome the issue, an assumption was made of 10 cm release diameter as a start.

Table 4: Gas Flowrates in Rotvoll Experiment in Nl/s, Nm^3/s, and m^3/s

Release Flowrate in Nl/s	**Release flowrate in Nm^3/s**	**Release Flowrate in m^3/s**
85	0.085	0.05
170	0.17	0.1
750	0.75	0.45

In this chapter, the Rotvoll Experiment is simulated to validate the general model designed for subsea gas releases. Three sets of simulations were conducted illustrated in Table 5, the simulation results will be compared against the experimental data to reach to most accurate model.

Table 5: Summary of all sets of simulations conducted

Set 1	Methane (const. density) release from **10 cm** diameter
Set 2	Methane (const. density) release from **17 cm** diameter
Set 3	Methane (ideal gas) release from **17 cm** diameter

7.1 Set 1: Methane (const. density) release from 10 cm diameter

As the inlet boundary condition is defined in ANSYS Fluent as velocity inlet. The velocity values were obtained from the experiment's flowrates shown in Table 6.

Table 6: Set 1 of ANSYS Fluent Simulations- 10 cm release diameter.

Diameter		**0.1**	**m**
Radius		**0.05**	**m**
Cases			
No.	**Flowrates m^3/s**	**Area of the Release m^2**	**Velocity = flowrate/area (m/s)**
1	0.05	0.008	6.4
2	0.1		12.7
3	0.45		57.3

The findings of each case will be presented as follows:

- Pressure contour map.
- Velocity and Volume fraction contour map. The data will be compared against the experimental results. The void fraction can be defined to be the fraction of the volume that is occupied by the gas phase.

7.1.1 Case 1 – 0.05 m^3/s release of Methane

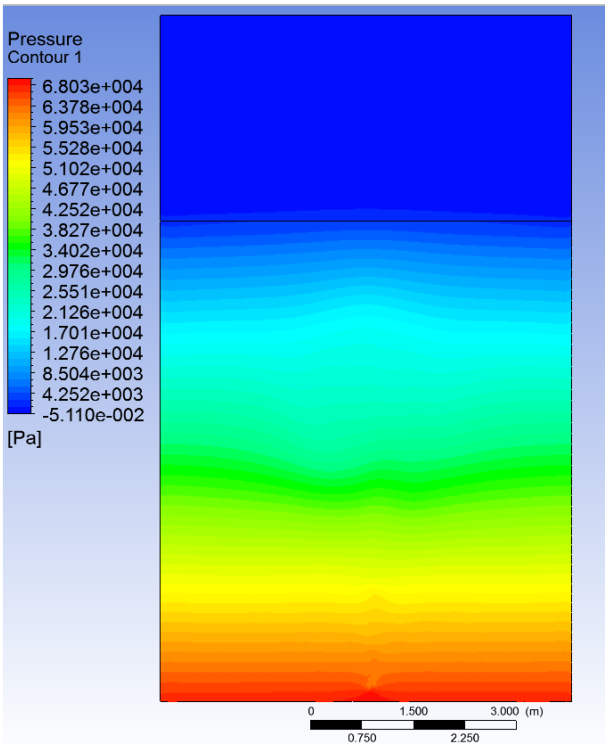

Figure 26: Pressure Contour map at the end of the release

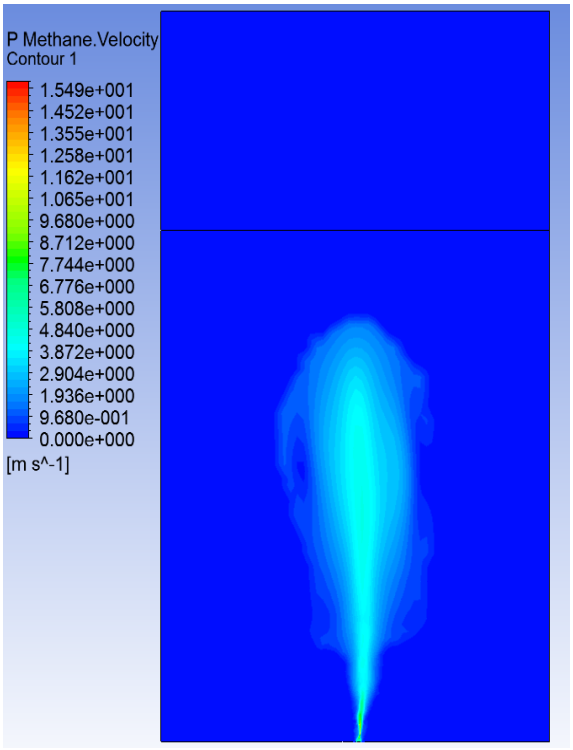

Figure 27: Velocity Contour Map after 4 seconds of the release

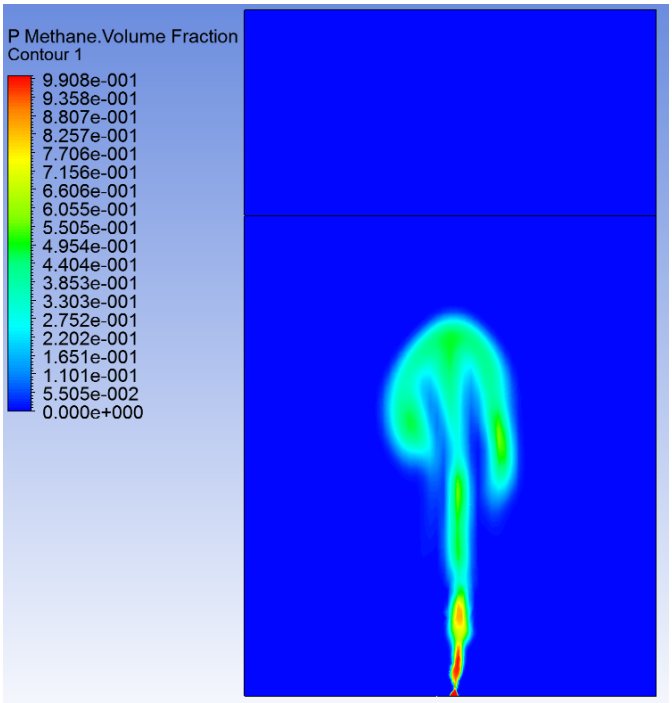

Figure 28: Volume Fraction Contour Map after 4 seconds of the release

The velocity and void fraction results were compared with the experimental data in Table 7 and Table 8 respectively.

Table 7: Simulation velocity results compared with the experimental data

Simulation	Experimental data for 0.05 m^3/ s		Error %
Centerline Velocity (m/s)	Centerline Velocity (m/s)	Vertical Distance (m)	
0.83	1.83	5.8	73
3.48	2.13	3.81	
4.35	2.17	1.76	

Table 8: Simulation void fraction results compared with the experimental data

Simulation	Experimental data for 0.05 m^3/ s		Error %
Void Fractions %	Void Fractions %	Vertical Distance (m)	
9.5	5.7	5.8	93
20	8.3	3.81	
22	13	1.76	

7.1.2 Case 2 – 0.1 m^3/s release of Methane

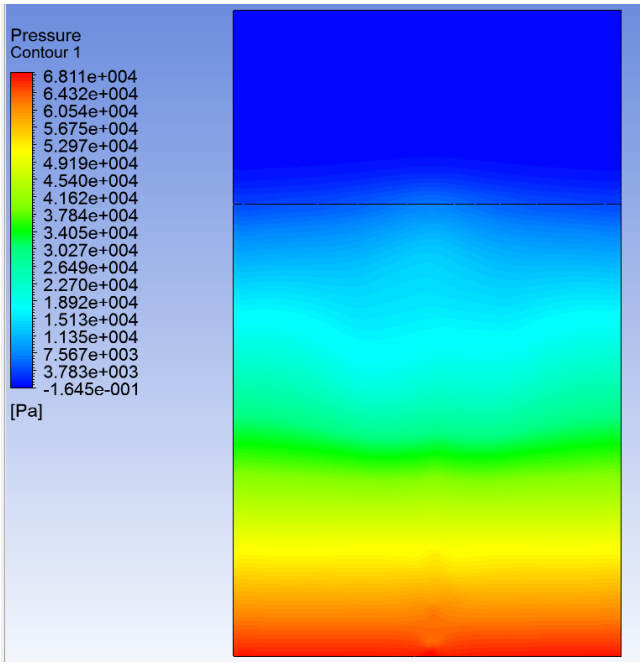

Figure 29: Pressure contour map

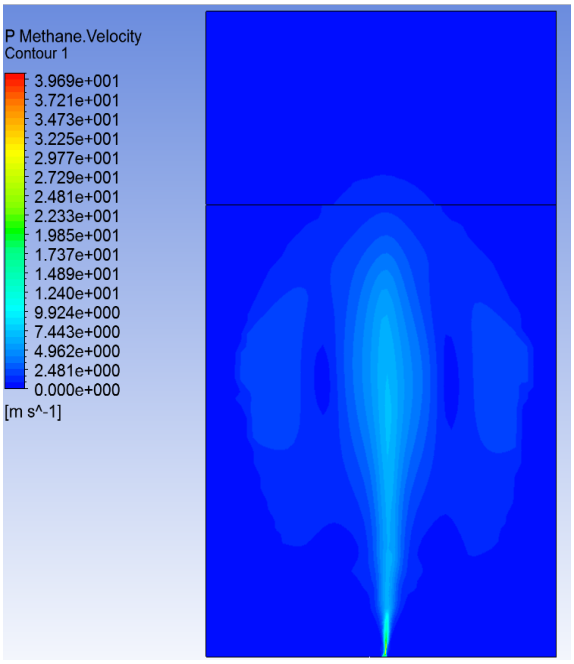

Figure 30: Velocity Contour Map directly

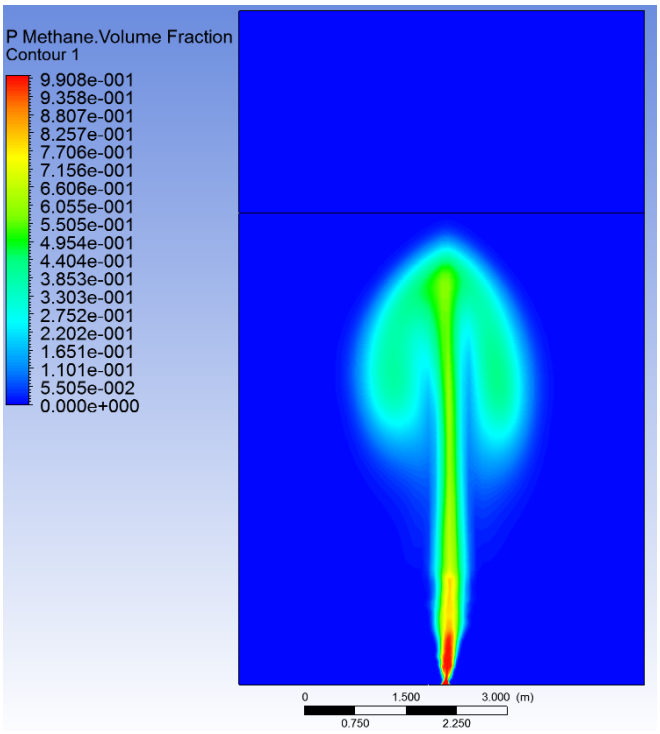

Figure 31: Volume Fraction Contour Map directly while reaching the surface

The velocity and void fraction results were compared with the experimental data in Table 9 and Table 10 respectively.

Table 9: Simulation velocity results compared with the experimental data

Simulation	Experimental data for 0.1 m^3/ s		Error %
Centerline Velocity (m/s)	Centerline Velocity (m/s)	Vertical Distance (m)	
2.481	2.1	5.8	48.9
3.722	2.43	3.81	
4.962	2.83	1.76	

Table 10: Simulation void fraction results compared with the experimental data

Simulation	Experimental data for 0.1 m^3/ s		Error %
Void Fractions %	Void Fractions %	Vertical Distance (m)	
12.1	8.3	5.8	205
50	11	3.81	
63	20	1.76	

7.1.3 Case 3 – 0.45 m^3/s release of Methane

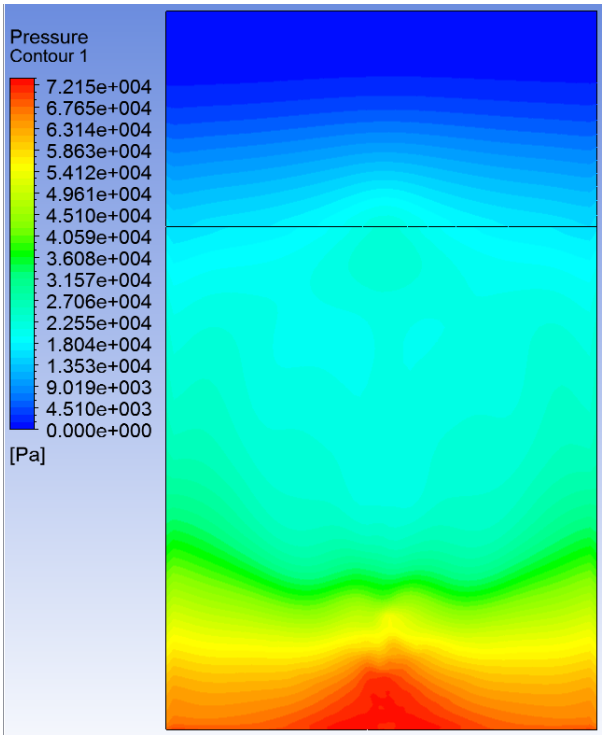

Figure 32: Pressure contour map

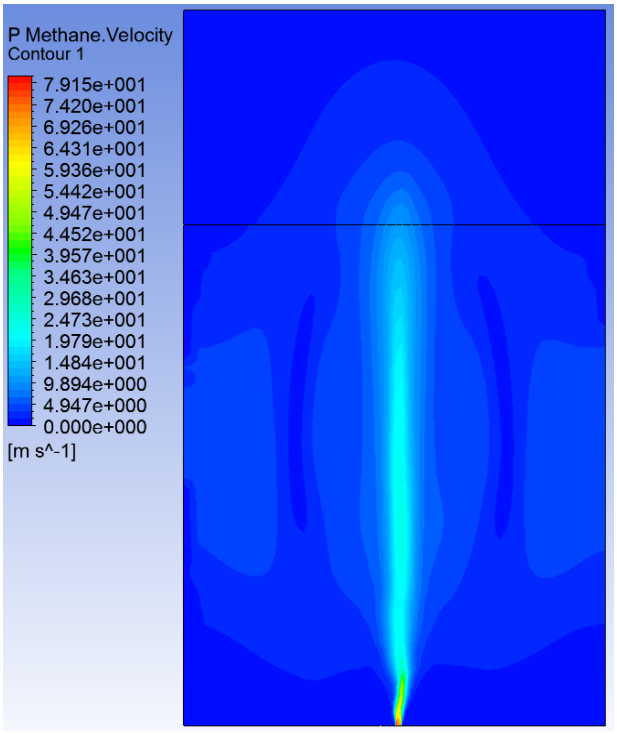

Figure 33: Velocity contour map

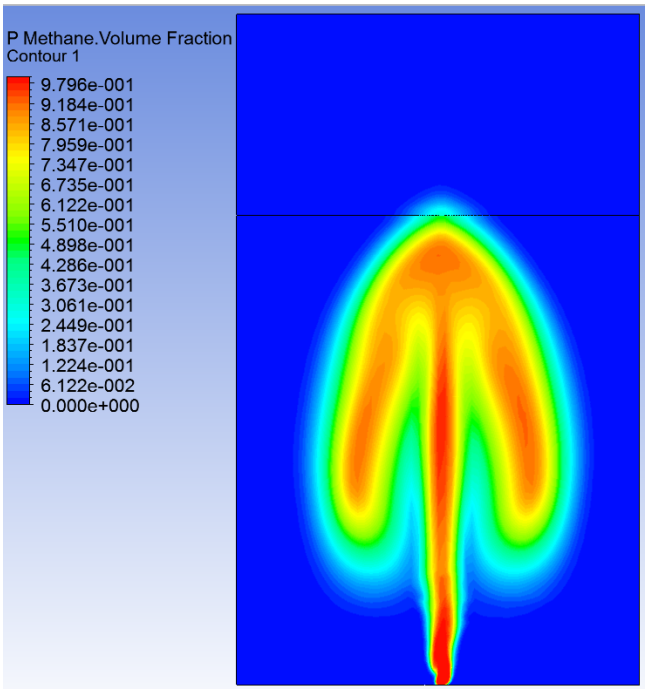

Figure 34: Void/Volume fraction contour map

The velocity and void fraction results were compared with the experimental data in Table 11.

Table 11: Simulation void fraction and velocity results compared with the experimental data

Simulation	**Experimental data for 0.45 m^3/ s**		**Error %**
Void Fractions %	**Void Fractions %**	**Vertical Distance (m)**	
38.5	20	5.8	83.5
Simulation	**Experimental data for 0.45 m^3/ s**		**Error %**
Centerline Velocity (m/s)	**Centerline Velocity (m/s)**	**Vertical Distance (m)**	
2.698	3.1	5.8	13.0

7.1.4 Discussion

The simulation data did not agree with the experimental results for both the velocity and the volume fractions as illustrated in Figure 35 and Figure 36.

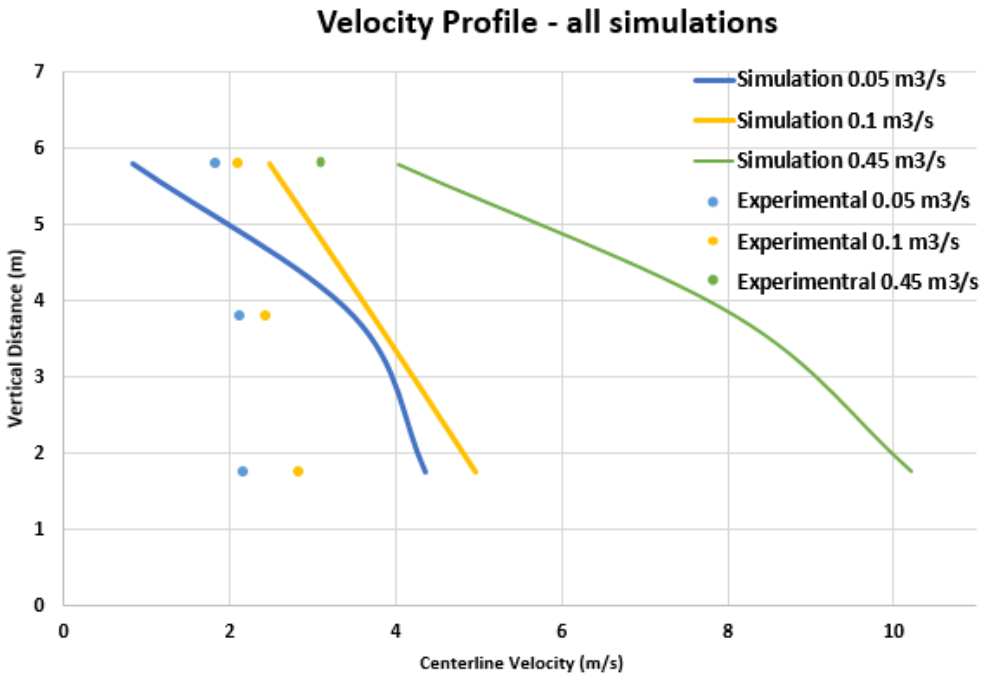

Figure 35: Experimental vs. Simulation Velocity profile for all simulations

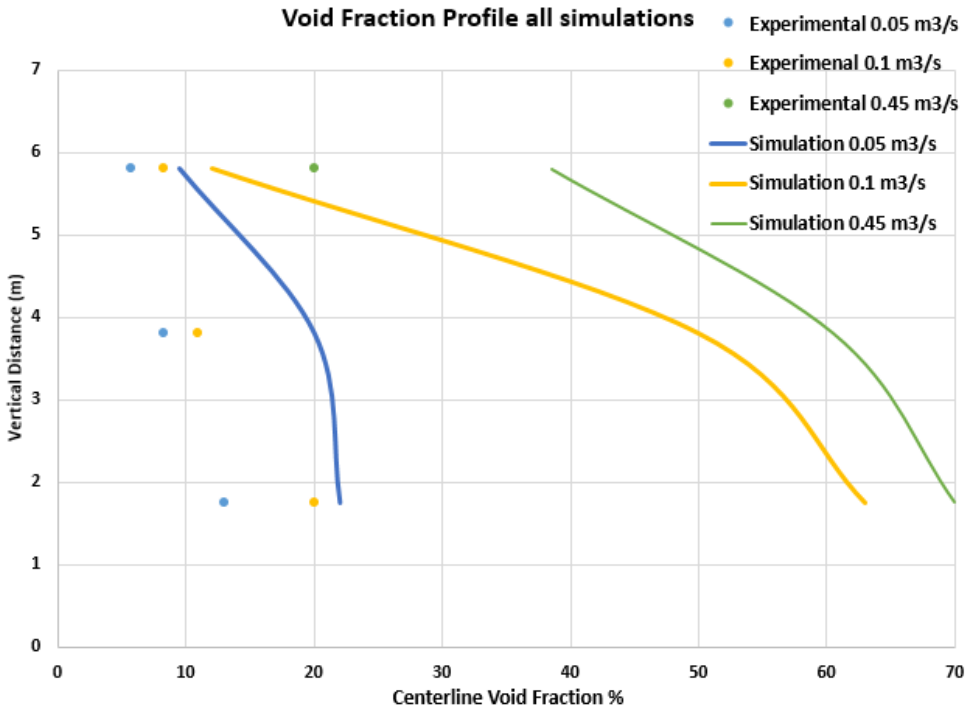

Figure 36: Experimental vs. Simulation volume fraction profile for all simulations

The errors are very high and this setup cannot be taken as a model for subsea gas releases. The Rise time parameter was checked and compared with the experimental rise time of the plume. The Rise time can be defined as the time it takes the first initiated bubble to reach to the water surface.

Table 12 shows the rise time for both the simulation and the experimental data. The error was found to be high as well for the different flowrates simulated. The design of the abovementioned model is not a representative for a subsea gas release by any means.

Table 12: Simulation and experimental rise time of the bubble plume

Flowrate m^3/s	Simulation Rise Time (sec)	Experiment Rise Time	Error %
0.05	4.6	6.0	23.3
0.1	3.3	4.8	31.3
0.45	2.03	3.1	34.5

After exploring many literature papers and reports by SINTEF, it was found that the exact release diameter was 17 cm, not the assumed 10 cm. The next set was conducted with the 17 cm release diameter by releasing the same flow rates of methane gas.

7.2 Set 2: Methane (const. density) release from 17 cm diameter

As done in Set 1, the Inlet Boundary Condition is defined in ANSYS Fluent as Velocity Inlet. The velocity values were obtained from the experiment's flowrates shown in Table 13.

Table 13: Set 2 of ANSYS Fluent Simulations- 17 cm release diameter

Diameter		**0.17**	**m**
Radius		**0.085**	**m**
Cases			
No.	**Flowrates m^3/s**	**Area of the Release m^2**	**Velocity = flowrate/area (m/s)**
1	0.05	0.023	2.2
2	0.1		4.4
3	0.45		19.8

The findings of each case will be presented as follows:

- Velocity and Volume fraction contour map. The data will be compared against the experimental results. The void fraction can be defined to be the fraction of the volume that is occupied by the gas phase.

The experimental velocity and void fraction data were recorded after the pseudo-steady-state flow is reached. There were no data available on the exact time required to reach to the pseudo-steady-state flow where the flow is stabilized with no fluctuation. However, in order to make achieve the pseudo-steady-state flow in the simulation, the methane was released up to 20 seconds. The data

were monitored and recorded every 0.01 seconds. Once the flow data are stabilized, the assumption of the pseudo-steady-state flow was set.

7.2.1 Case 1 – 0.05 m^3/s release of Methane

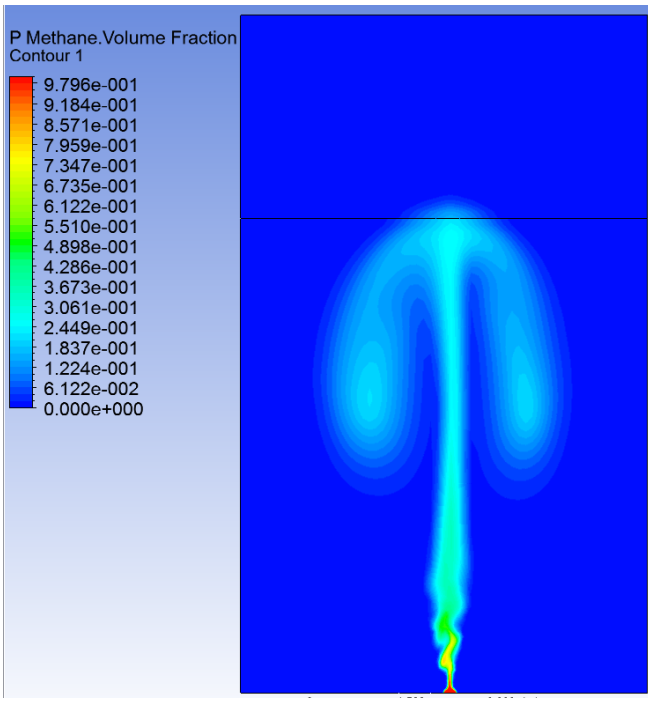

Figure 37: Methane Volume Fraction counter map

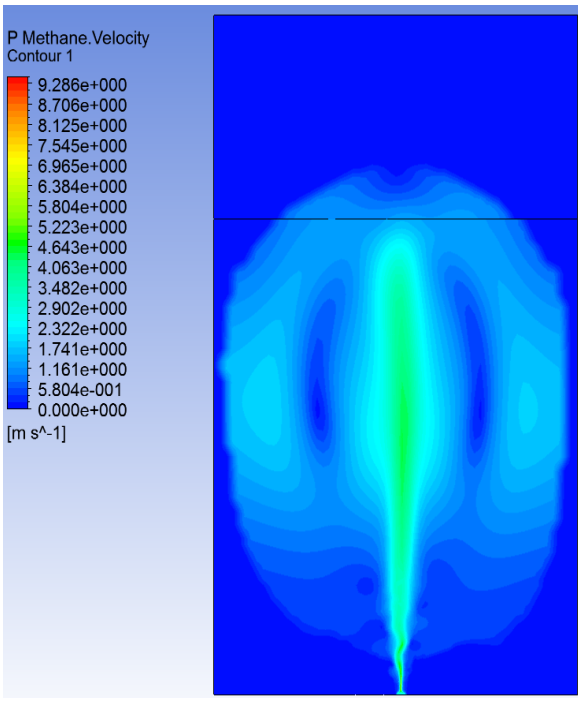

Figure 38: Methane velocity counter map

The pseudo-steady-state condition was reached in the 0.05 m^3/s methane release after 11.5 seconds. The velocity and void fraction results were compared with the experimental data in Table 14 and Table 15 respectively.

Table 14: Simulation velocity results compared with the experimental data

Simulation	Experimental data for 0.05 m^3/ s		Average Error %
Centerline Velocity (m/s)	Centerline Velocity (m/s)	Vertical Distance (m)	
2.8	1.83	5.8	57.9
3.3	2.13	3.81	
3.6	2.17	1.76	

Table 15: Simulation void fractions results compared with the experimental data

Simulation	Experimental data for 0.05 m^3/ s		Error %
Void Fractions %	Void Fractions %	Vertical Distance (m)	
11	5.7	5.8	87.0
16.5	8.3	3.81	
22	13	1.76	

7.2.2 Case 2 – 0.1 m^3/s release of Methane

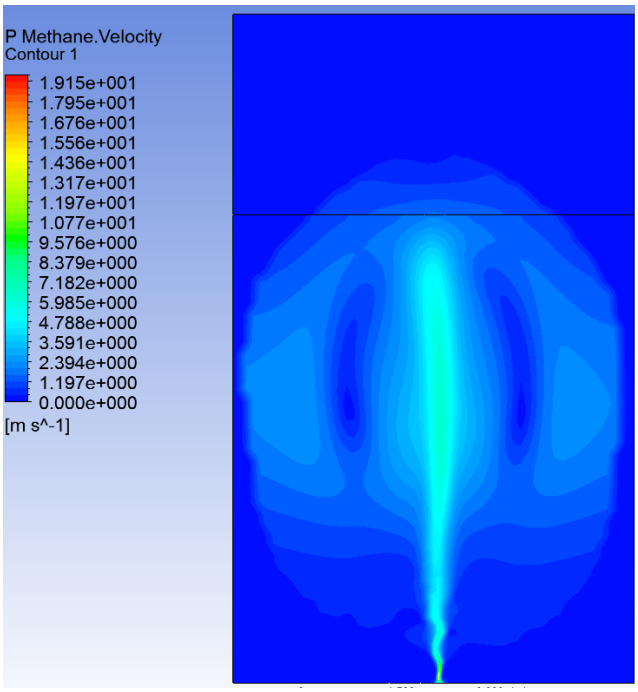

Figure 39: Velocity contour map

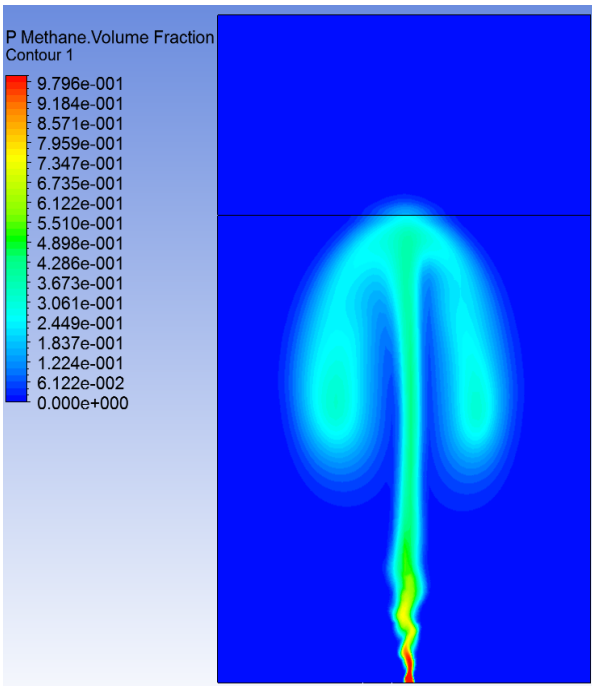

Figure 40: Volume Fraction of methane contour map

The pseudo-steady-state condition was reached in the 0.1 m^3/s methane release after 14.2 seconds. The velocity and void fraction results were compared with the experimental data in Table 16 and Table 17 respectively.

Table 16: Simulation velocity results compared with the experimental data

Simulation	Experimental data for 0.1 m^3/ s		Error %
Centerline Velocity (m/s)	Centerline Velocity (m/s)	Vertical Distance (m)	
2.92	2.1	5.8	48.7
3.6	2.43	3.81	
4.5	2.83	1.76	

Table 17: Simulation void fraction results compared with the experimental data

Simulation	Experimental data for 0.1 m^3/ s		Error %
Void Fractions %	Void Fractions %	Vertical Distance (m)	
22	8.3	5.8	125.2
27	11	3.81	
33	20	1.76	

7.2.3 Case 3 – 0.45 m^3/s release of Methane

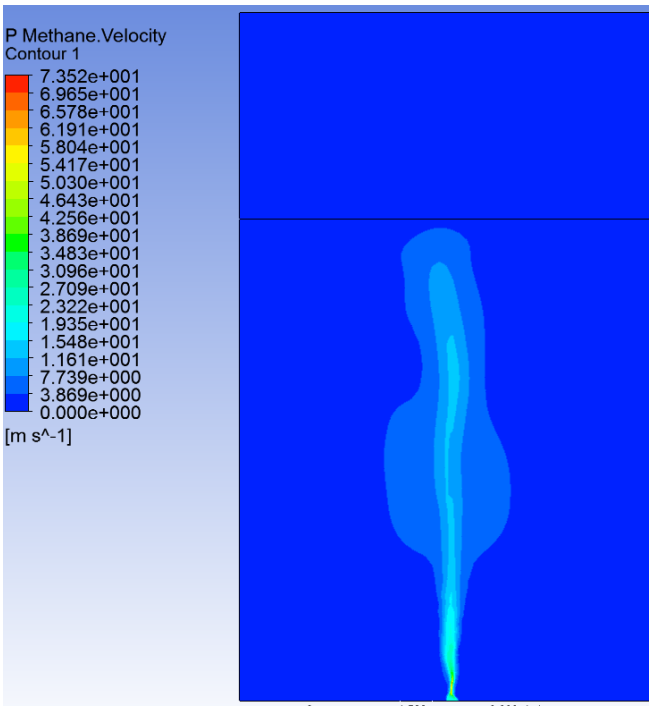

Figure 41: Velocity Contour Map

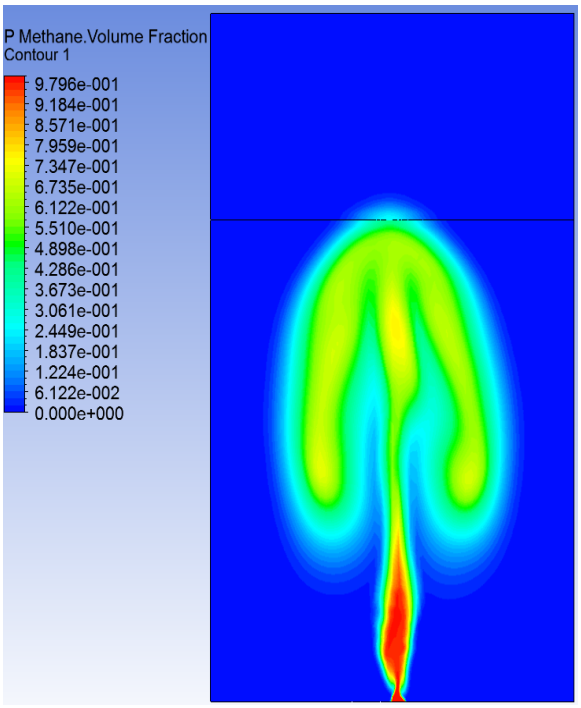

Figure 42: Volume Fraction contour map

The pseudo-steady-state condition was reached in the 0.45 m^3/s methane release after 5.1 seconds.

The velocity and void fraction results were compared with the experimental data in Table 18.

Table 18: Simulation void fraction and velocity results compared with the experimental data

Simulation	**Experimental data for 0.45 m^3/s**	
Void Fractions %	**Void Fractions %**	**Vertical Distance (m)**
27.5	20	5.8
Simulation	**Experimental data for 0.45 m^3/s**	
Centerline Velocity (m/s)	**Centerline Velocity (m/s)**	**Vertical Distance (m)**
5.4	3.1	5.8

7.2.4 Discussion

As the flow rate increases, the force resulted from buoyancy, turbulence and the drag force increase which entrains the liquid upward. In addition to the increase in the horizontal dispersion of the gas in the water body. The higher the flow rate, the less time taken to reach to the surface.

As can be seen in both Figure 43 and Figure 44, the velocity and volume fraction simulation results are compared with the experimental data.

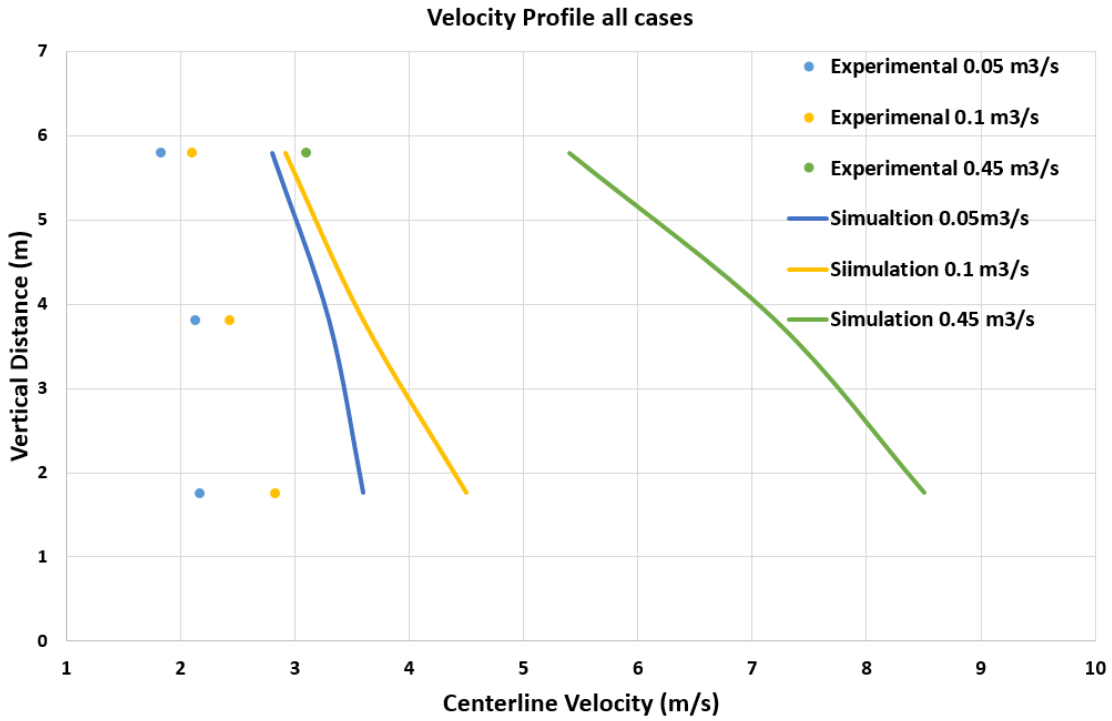

Figure 43: Experimental vs. Simulation Velocity profile for all simulations

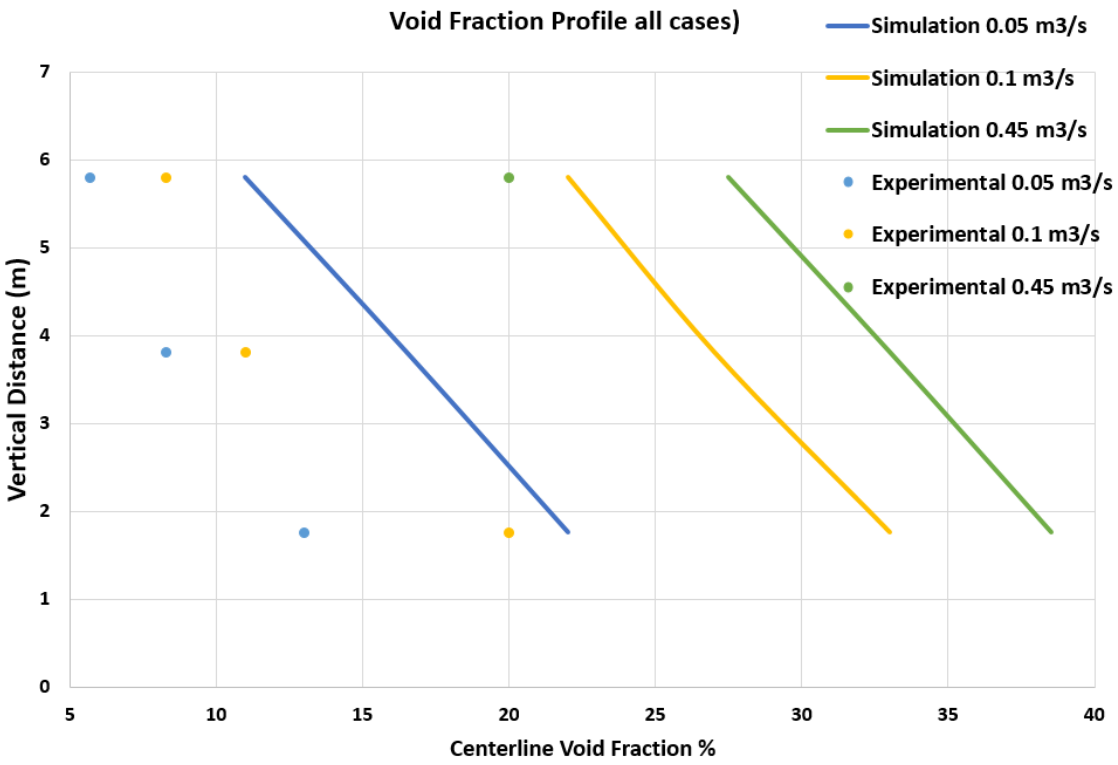

Figure 44: Experimental vs. Simulation volume fraction profile for all simulations

The velocity and methane volume fraction results show an improvement compared to the 10 cm case with the experimental data with an average error of approximately 45 % compared to 73 % in the previous set for velocity measurements. The error values are still too high and not acceptable for the methane volume fraction measurements. The wrong predictions of velocity and volume fractions in case of the high flow rate scenarios had a big contribution in the error resulted and it is unlikely to be ignored. The rise time data are reported for the 3 cases in

Table 19. The rise time for the 3 cases is approximately 1 second earlier compared to the experimental rise time.

Table 19: Rise Time data

Flowrate m^3/s	Simulation Rise Time (sec)	Experiment Rise Time
0.05	5.04	6.0
0.1	3.9	4.8
0.45	2.32	3.1

The density of the gas changes as the depth increases. In order to simulate a real release of gas, the equation of state should be activated in ANSYS Fluent to account for the change in released gas density. For the shallow depths, the ideal gas law is to be used [2].

One possible cause of the big error resulted is that the inlet boundary condition was selected as a velocity inlet to release the methane with a certain velocity in each case. Velocity inlet boundary condition is used in case of incompressible flows. This type of inlet is intended to be used for the incompressible flows. In this type of inlets, the flow properties vary to accommodate for the prescribed velocity distribution. Using the velocity inlet, in case of the compressible flows can lead to wrong predictions and non-physical results. In addition, placing the velocity inlet in small geometries or near walls may have a great effect on the solution. The mass flow inlet boundary type is used in the compressible flows scenarios to prescribe mass flow rate at inlet [53].

The suggested solution to overcome the volume fraction issue was to let the methane gas behave as an ideal gas law. In addition, the inlet boundary conditions will be changed to mass flow inlet. The next set will simulate the same three simulations done in this section but with assuming that the density of methane will follow the ideal gas law.

7.3 Set 3: Methane (ideal gas) release from 17 cm diameter

The inlet boundary condition is defined in ANSYS Fluent as Mass flow inlet. Three simulations were conducted according to Table 20.

Table 20: Set 3 of ANSYS Fluent Simulations- 17 cm release diameter

Diameter		**0.17**	**m**
Radius		**0.085**	**m**
Cases			
No.	**Flowrates m^3/s**	**Area of the Release m^2**	**Mass flowrates kg/s**
1	0.05	0.023	0.03
2	0.1		0.06
3	0.45		0.3

The findings of each case will be presented as follows:

- Velocity and volume fraction contour map. The data will be compared against the experimental results. The void fraction can be defined to be the fraction of the volume that is occupied by the gas phase.

The released methane will be simulated as an ideal gas. There are some parameters defined for the other phases before simulating the three cases according to the following:

The density of the water phase = $998.2 \frac{kg}{m^3}$

The viscosity of the water phase = $0.001003 \frac{kg}{m.s}$

A uniform temperature distribution was assumed to be equal $= 15$ ℃

The air density was specified = $1.225 \frac{kg}{m^3}$

The viscosity of the air = $1.7894 \times 10^{-5} \frac{kg}{m.s}$

The density distribution of the methane gas will follow the ideal gas behavior. For shallow waters as indicated in chapter 2, the assumption of the ideal gas will be assumed and then the density can be defined as the following:

$$\boldsymbol{P_l M_w = \rho R_g T}$$ Equation 38

Where P_l can defined as the hydrostatic pressure of the surrounding water, R_g is the gas constant and T_l is the temperature of the surrounding water.

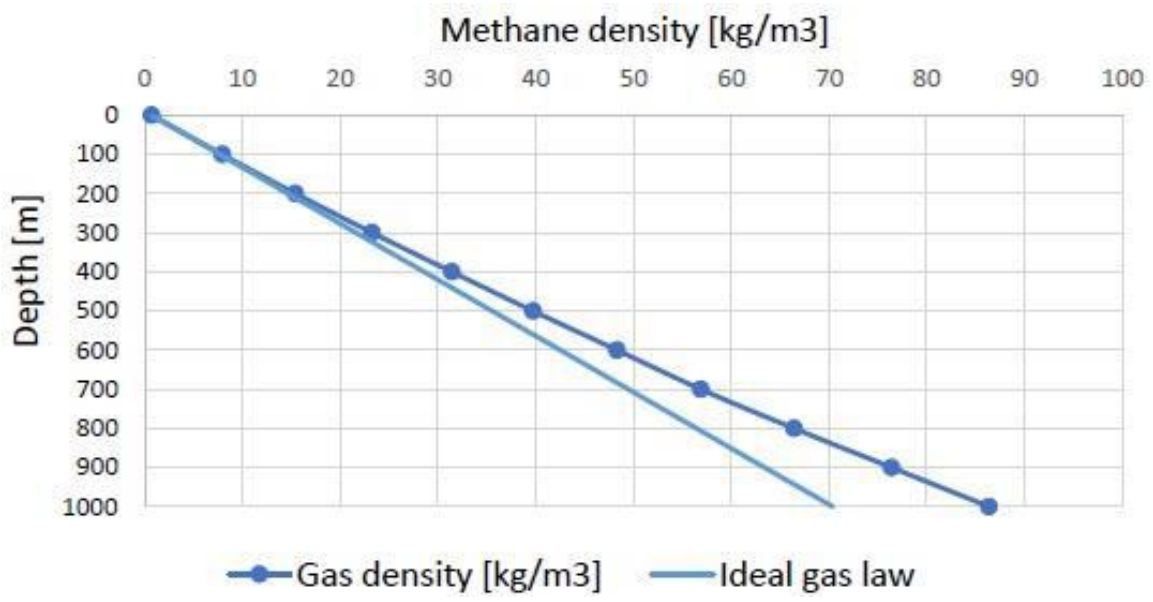

Figure 45: Methane ideal gas density as a function of the depth [54]

Figure 45 shows the methane gas density using the ideal gas law as a function of depth at 25^{o}C [54]. The effect of the non-ideality is negligible in this thesis.

7.3.1 Case 1 – 0.05 m^3/s release of Methane

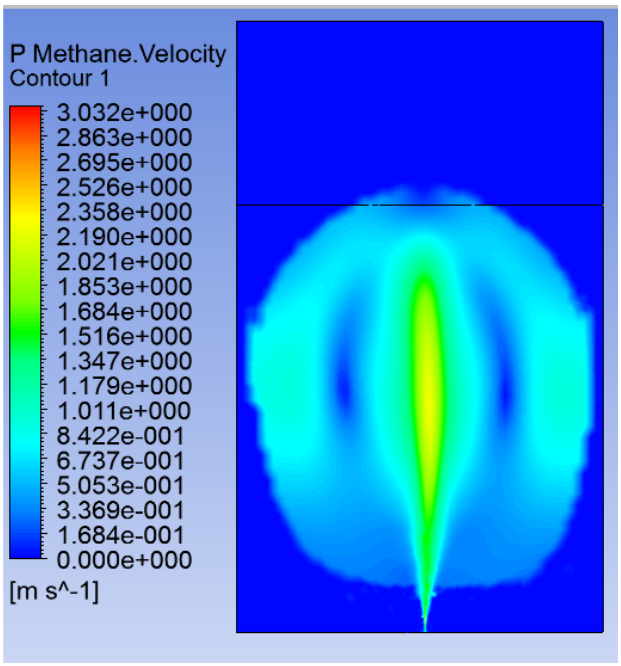

Figure 46: Velocity contour map

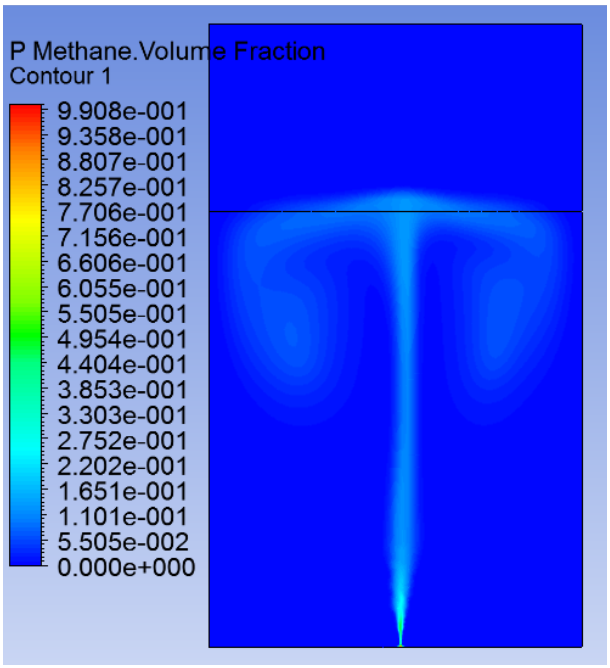

Figure 47: Methane volume fraction contour map

The velocity and void fraction results were compared with the experimental data in Table 21 and Table 22 respectively.

Table 21: Simulation velocity results compared with the experimental data

Simulation	Experimental data for 0.05 m^3/ s		Average Error %
Centerline Velocity (m/s)	Centerline Velocity (m/s)	Vertical Distance (m)	
1.85	1.83	5.8	2.5
2.19	2.13	3.81	
2.25	2.17	1.76	

Table 22: Simulation void fractions results compared with the experimental data

Simulation	Experimental data for 0.05 m^3/ s		Average Error %
Void Fractions %	Void Fractions %	Vertical Distance (m)	
6.3	5.7	5.8	18.0
10	8.3	3.81	
16	13	1.76	

7.3.2 Case 2 – 0.1 m^3/s release of Methane

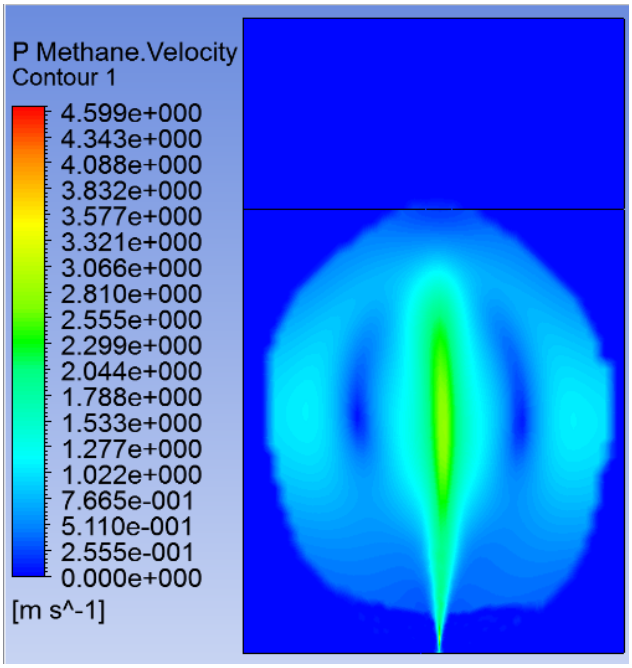

Figure 48: Velocity contour map

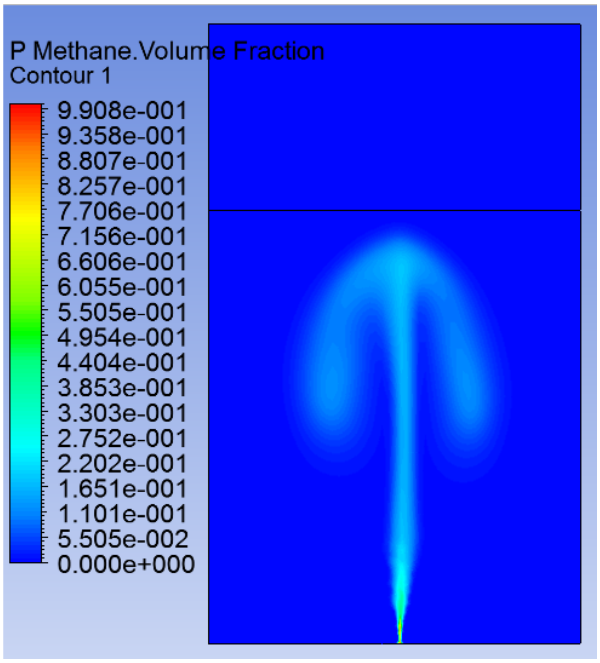

Figure 49: Volume Fraction contour map

The velocity results were compared with the experimental data in Table 23 and Table 24.

Table 23: Simulation velocity results compared with the experimental data

Simulation	**Experimental data for 0.1 m^3/ s**		**Average Error %**
Centerline Velocity (m/s)	**Centerline Velocity (m/s)**	**Vertical Distance (m)**	
2.17	2.1	5.8	2.1
2.5	2.43	3.81	
2.83	2.83	1.76	

Table 24: Simulation volume fraction results compared with the experimental data

Simulation	**Experimental data for 0.1 m^3/ s**		**Average Error %**
Void Fractions %	**Void Fractions %**	**Vertical Distance (m)**	
8.3	8.3	5.8	2.5
11	11	3.81	
21	20	1.76	

7.3.3 Case 3 – 0.45 m^3/s release of Methane

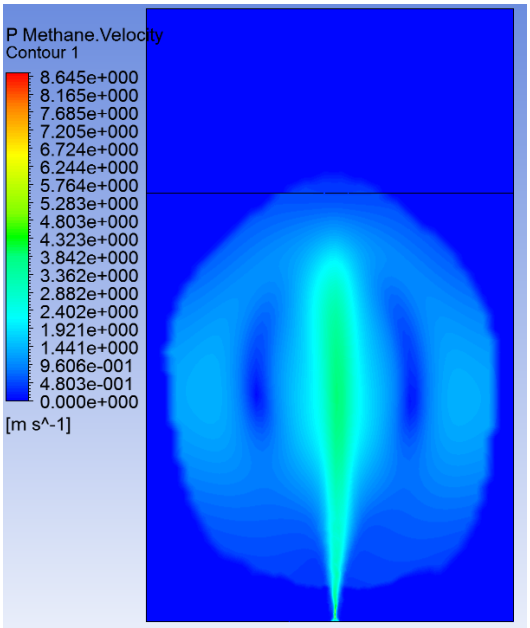

Figure 50: Velocity contour map

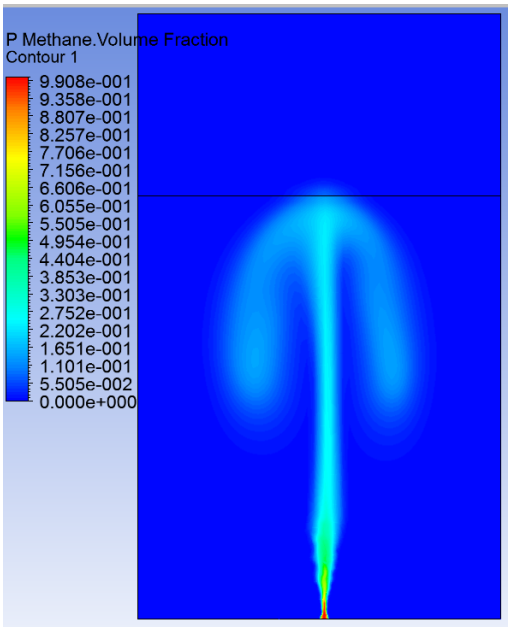

Figure 51: Volume fraction contour map

The velocity and void fraction results were compared with the experimental data in Table 25.

Table 25: Experimental and simulation data for both the void fractions and the velocity

Simulation	**Experimental data for 0.45 m^3/s**		**Error %**
Void Fractions %	**Void Fractions %**	**Vertical Distance (m)**	
21	20	5.8	5.0
Simulation	**Experimental data for 0.45 m^3/s**		**Error %**
Centerline Velocity (m/s)	**Centerline Velocity (m/s)**	**Vertical Distance (m)**	
3.3	3.1	5.8	6.5

7.3.4 Surface Zone

In the free water surface zone, the movement of the rising water is different. The rising water deflected in a radial movement upon reaching the surface zone due to the momentum of the entrained water plume as shown in Figure 52. The figure shows the elevation of the water surface leading to a formation of the water fountain. The vectors indicate the radial movement and the formation of the water fountain while the gas is escaping to the atmosphere.

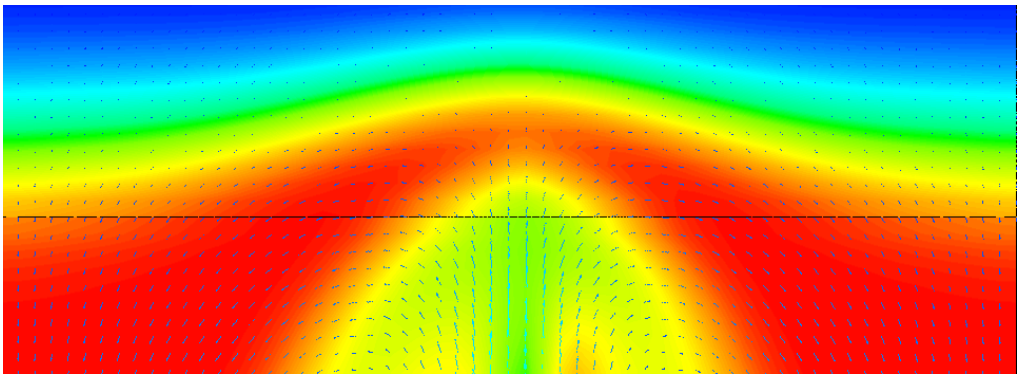

Figure 52: Vector contour plot colored by the volume fractions at the free water surface

7.3.5 Discussion

As the flow rate increases, the force resulted from buoyancy, turbulence and the drag force increases which entrains the liquid upward. The higher the flow rate, the less time taken to reach to the surface.

Both Figure 53 and Figure 54 show the velocity and the volume fraction profiles for different flow rates. The velocity and volume fraction simulation results are compared against the experimental data and the simulation results by the first SINTEF subsea gas release model.

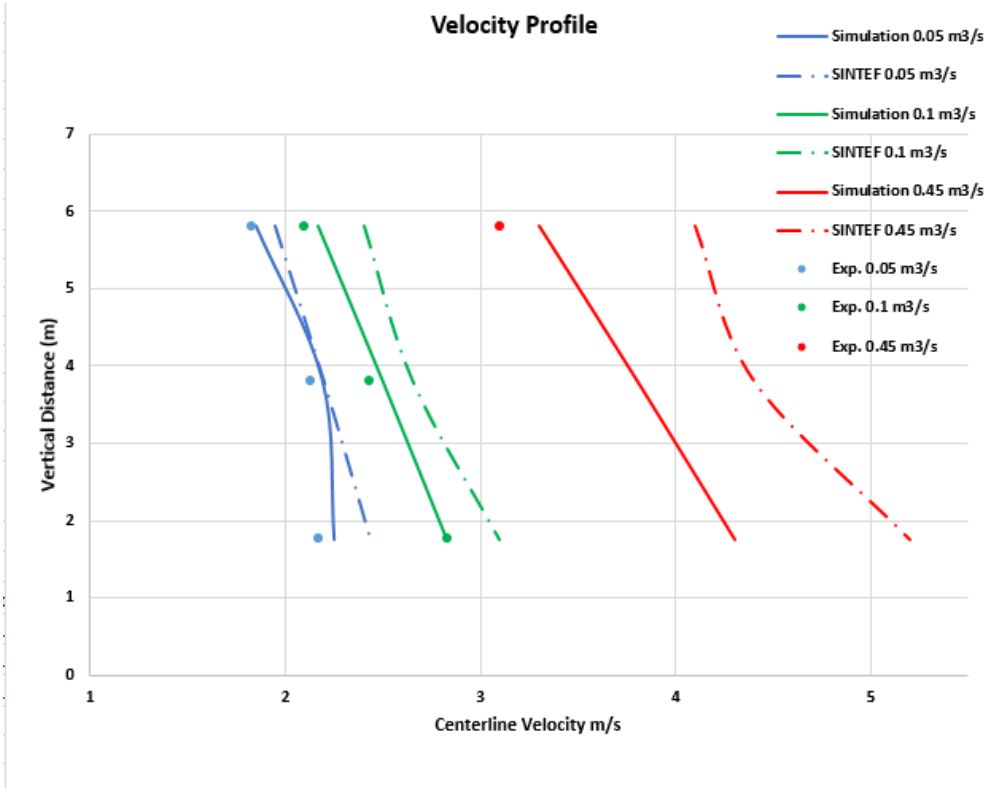

Figure 53: Simulation results vs experimental data compared to the simulation results from SINTEF model for velocity profile

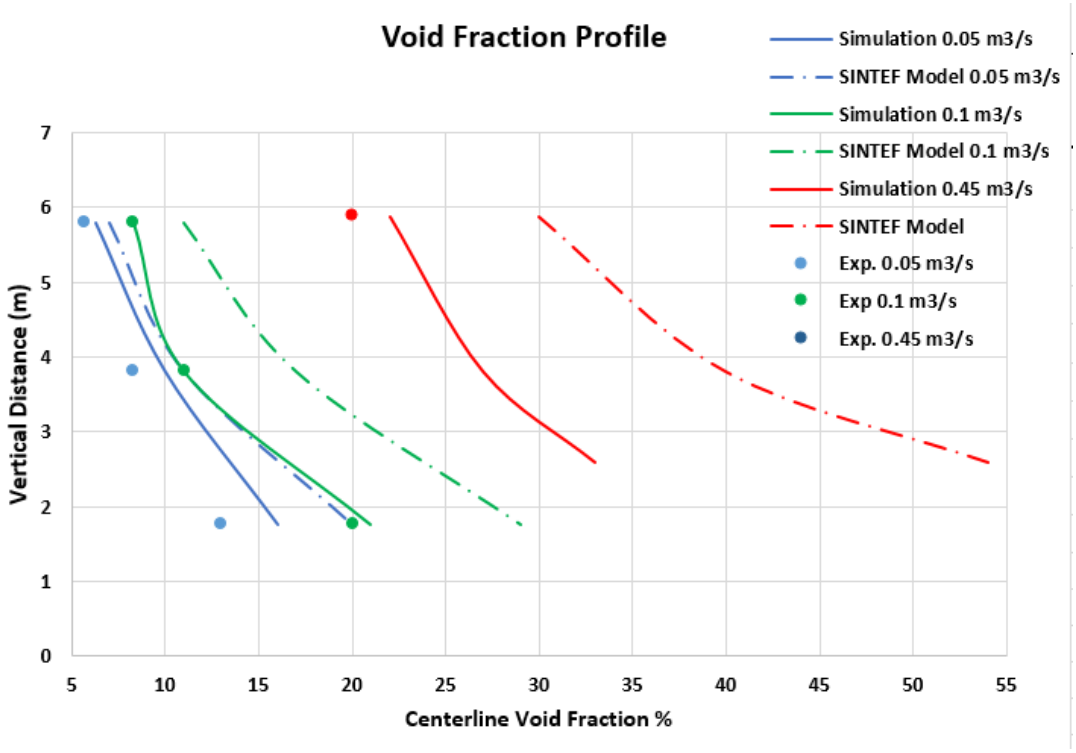

Figure 54: Simulation results vs experimental data compared to the simulation results from SINTEF model for void fraction profile

The velocity and volume fractions simulation results show an excellent agreement with the experimental data in Figure 53 and Figure 54 with an average error of 2 % and 8.5 % respectively. The simulation results follow the same behavior as the experimental data. Unlike the results from the SINTEF model, the errors are very high compared to our developed model and the model fails to predict accurate data on the surface. The improvements implemented (e.g. RNG $k-\varepsilon$ model and mass flow inlet boundary condition) had a great impact on the accuracy reached.

The RNG $k-\varepsilon$ model proved its efficiency in modeling strained/high flows. This is due to the extra terms added to its equations that accounted for swirl motions resulted from the high turbulence and the behavior near the near-wall region and the surface interactions [55].

The rise time data were reported for the 3 cases in Table 26, the rise time for the 3 cases matches exactly the experimental rise time.

Table 26: Rise Time data

Flowrate m^3/s	**Simulation Rise Time (sec)**	**Experiment Rise Time**
0.05	5.4	6.0
0.1	4.8	4.8
0.45	3.2	3.1

The improvements implemented in this set were sufficient to get an accurate model. The model setup can be used sufficiently to model subsea gas releases in shallow waters. The model will be extended to model subsea releases in different shallow water depths and different releases diameters and flow rates related to Qatar's offshore industry.

8 50 METERS SIMULATIONS

The main objective of this project was to develop a general model for shallow waters subsea gas releases. The model was developed and verified against Rotvoll experimental data in the previous chapters. Figure 18 illustrates the range that the previous experiments covered. Compared to the flowrates and depths associated with the offshore industry, the experimental data provides very limited information to be used in the risk assessment. SINTEF had proposed a depth/rate range of concern showed in Figure 18 that should be investigated and analyzed [2].

The aim is to create a database by simulating most of the scenarios in the range of concern to get an insight on the behavior of the bubble plume when a subsea release occurs. The developed model in the previous chapter proved its reliability in predicting the behavior of bubble plume in subsea gas releases in shallow waters. The model will be extended to simulate different methane flowrates from the range of the concern. The new geometry will be a representation of the Arabian Gulf waters with a depth of 50 m.

Three Scenarios were defined to be simulated using the developed CFD model shown in Table 27. The diameter of release was assumed to 25 cm to start the first set of simulations. Three simulations were defined for this set of simulations [50].

Table 27: Scenarios defined to be simulated using the developed CFD model

Case No.	Mass flowrate (kg/s)
1	20
2	50
3	100

8.1 Model Setup – Depth Modification

The model was modified by extending the water body depth to 50 m, the air body depth to 5 m and the release diameter was changed to 25 cm illustrated in Figure 55.

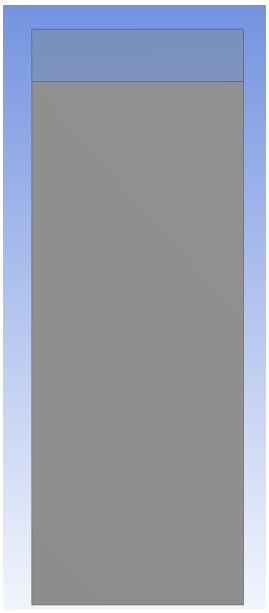

Figure 55: Modification of the geometry

The mesh was updated automatically by the meshing in the ANSYS Workbench. The simulation was performed with 113838 quadrilaterals cells.

The simulation setup is ready to edit the flow properties and set the initial and the boundary conditions. The chemical and physical properties were kept the same except the mass flow rate inlet condition. It was varied according to Table 28.

8.2 Set 1: Methane release from 25 cm diameter in 50 m depth

The inlet boundary condition is defined in ANSYS Fluent as Mass flow inlet. Three simulations were conducted according to Table 28.

Table 28: Set 1 of ANSYS Fluent Simulations- 25 cm release diameter.

Diameter		**0.25 m**
Radius		**0.125 m**
No.	**Mass Flowrates m^3/s**	**Area of the Release m^2**
1	20	0.049
2	50	
3	100	

The findings of each case will be presented as follows:

- Volume fraction contour map.
- Rise Time

The simulation was done using the Supercomputer Hardware RAAD2 at Texas A&M University at Qatar. The simulation was run using 48 CPUs (12 times the normal computer) and each simulation took around 44 hours to converge.

It has been found that the surrounding pressure at the release point is approximately 5 bar. A non-chocked / chocked test was conducted to check if the flow behavior.

The following equations was used and the results are shown in

Table 29.

$$Q_m = C_0 A P_0 \sqrt{\frac{\gamma M}{R T_0} \left(\frac{2}{\gamma + 1}\right)^{\frac{\gamma+1}{\gamma-1}}}$$

Table 29: Chocked / non-chocked flow test

Temperature (°C)	Diameter (m)	Area (m^2)	P_0 (Pa)	Discharge coefficient C_o	P choked (Pa)	Q_m chocked (kg/s)
15	0.25	0.049	5.00E+05	0.61	2.71E+05	25.96

It was found that starting from a flowrate of 26 kg/s, the flow will be chocked. The flow can be referred to as supersonic.

8.2.1 Case 1 & 2 – 20 kg/s & 50 kg/s release of Methane

Figure 56 and Figure 57 show the volume fraction contour maps of 20 kg/s and 50 kg/s release of methane from 25 cm hole in a 50 m depth water body.

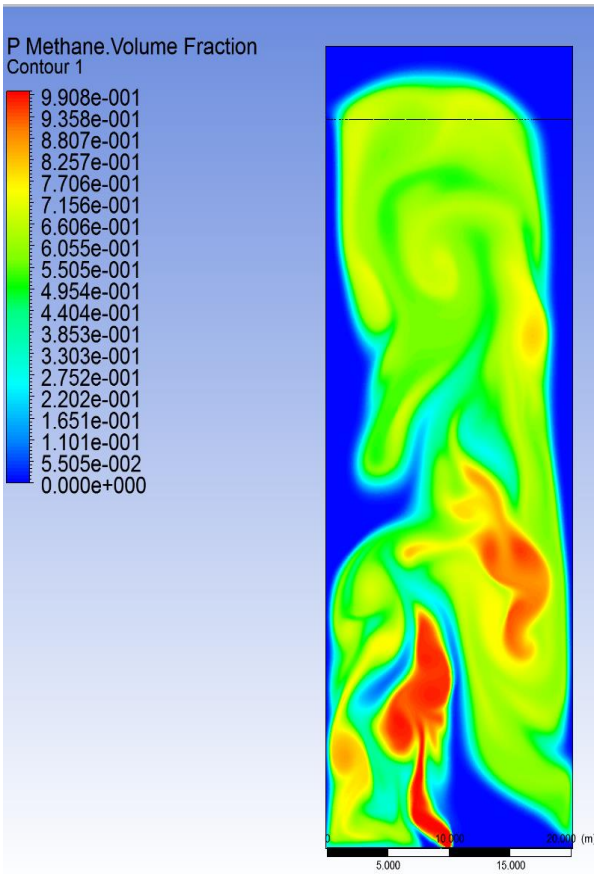

Figure 56: Volume fraction contour map for 20 kg/s

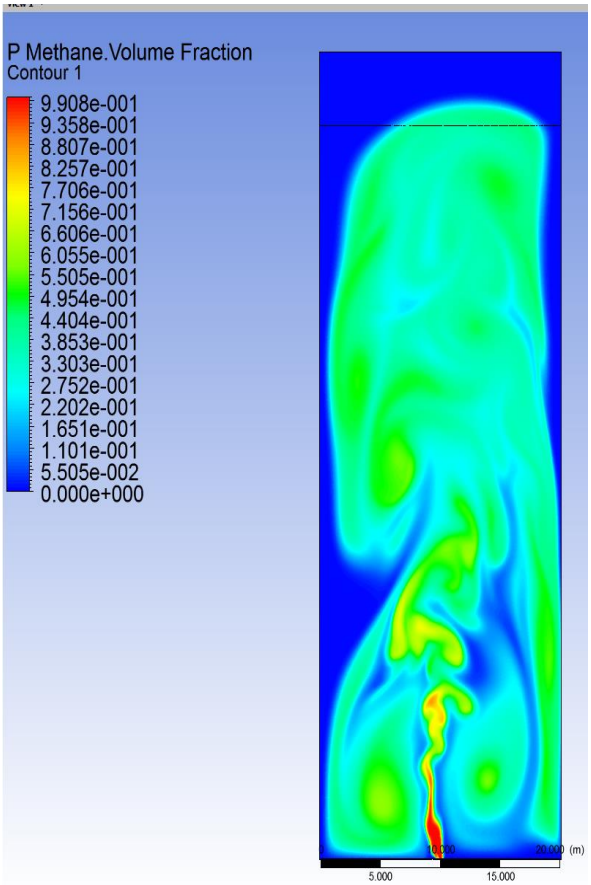

Figure 57: Volume fraction contour map for 50 kg/s

8.2.2 Case 3 – 100 kg/s release of Methane

Figure 58 shows the volume fraction contour map of 100 kg/s release of methane from 25 cm hole in a 50 m depth water body.

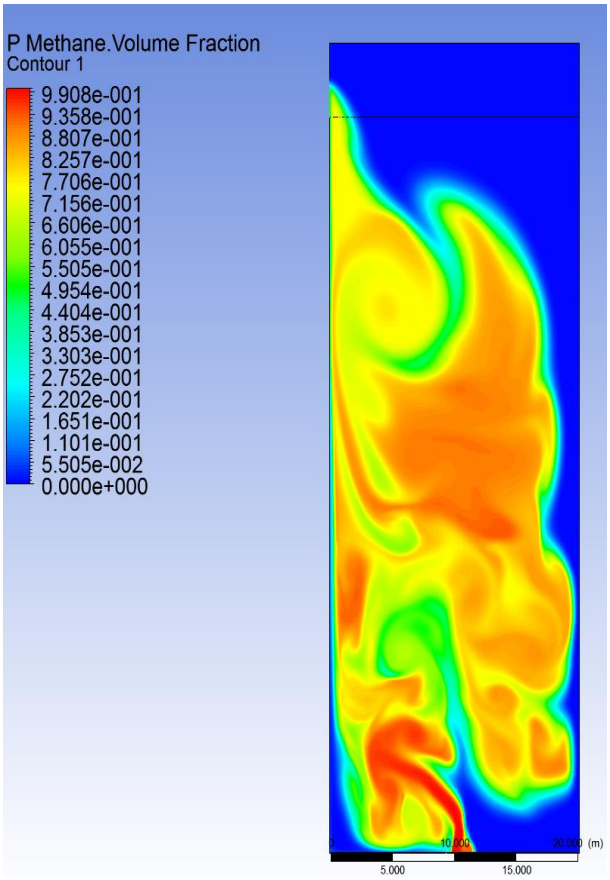

Figure 58: Volume fraction contour map for 100 kg/s

8.2.3 Discussion

The contour maps of the simulation were presented in the above sections. The verification of the model in the last chapter gave an insight of the reliability of the model to predict the subsea gas releases in shallow waters. Refer to Appendix 2 for velocity contour maps. The velocity decreases as moving upward. The velocity remains constant after it reaches to the middle of the geometry as the force exerted from the release vanished. This is where the diffusion of the bubble plume starts in the sea. As can be seen in the volume contour maps, the gas is diffusing in the water body reaching the edges and escaping to the surface, unlike the 7 m depth scenario where the diffusion was unlikely to occur. If the first case is to be considered as a real offshore scenario. If methane was released from a 25 cm hole at 20 kg/s, only 27 % of the released gas will escape to the surface. A similar investigation was done for the other cases. 30 to 40 % of the released gas will escape to the surface. The rise time data were recorded for the three simulations in Table 30.

Table 30: Rise Time

Mass flowrate kg/s	Simulation Rise Time (sec)
20	12
50	8
100	5

There are several parameters that are important for safety assessments and must be determined and reported as,

- Rise time
- Percentage of the gas escaped the water body
- Surface flux: which is going to be the input for the dispersion model used to analyze the surface.

These results were generated and presented in Table 31.

Table 31: Parameters estimated from 50 m simulations

Flowrate kg/s	Simulation Rise Time (sec)	Methane Percentage on the surface %	Mass Flux ($kg/m^2.s$)
20	12	27	0.035
50	8	33	0.109
100	5	40	0.415

It is believed that the random shape generated in the volume fraction contours were due to the high resolution of the mesh. The geometry was divided into more than 116 k nodes which is too high. A mesh study must be conducted to adjust the mesh to be more focused on the predicted shape of the bubble plume. The width of the geometry plays an important role in the dispersion of methane as methane collapse onto the wall and disperse back to the water body. It is believed that this geometry is not a representation of an offshore subsea gas release. It is suggested to reduce the

element size and increase the width of the geometry to 50 m to eliminate the effect of the walls on the dispersed gas. The geometry will be edited and the same flowrates will be released.

8.3 Set 2: Methane release from 25 cm diameter- modified geometry

The model was modified by extending the water body's width to 50 m, the air body's depth to 10 m and the release diameter was kept as 25 cm. The mesh was generated by reducing the element size to 50 cm. The simulation was performed with 16k quadrilaterals cells. The inlet boundary condition is defined in ANSYS Fluent as Mass flow inlet. The same flowrates were tested again using the new geometry. The findings of each case will be presented as follows:

- Volume fraction contour map.
- Rise Time

The simulation was done using the Supercomputer Hardware RAAD2 at Texas A&M University at Qatar. The simulation was run using 48 CPUs (12 times the normal computer) and each simulation took around 33 hours to converge.

8.3.1 Case 1 & 2 – 20 kg/s & 50 kg/s release of Methane

Figure 59 and Figure 60 show the volume fraction contour maps of 20 kg/s and 50 kg/s releases of methane from 25 cm hole in the modified geometry.

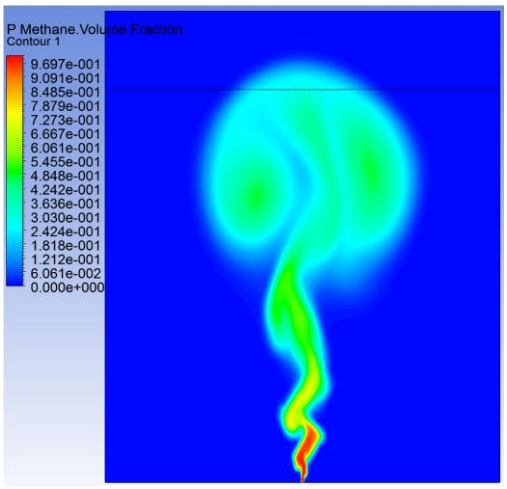

Figure 59: Volume fraction for 20kg/s

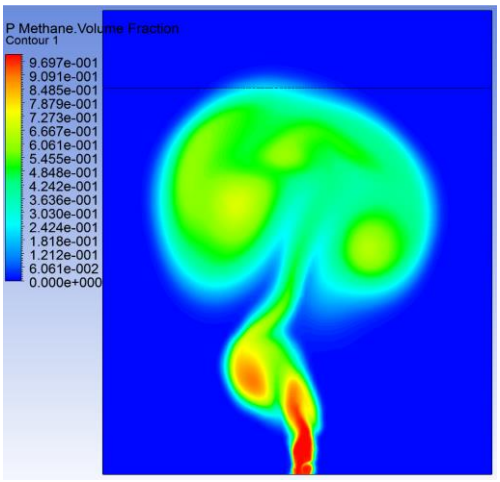

Figure 60: Volume fraction for 50 kg/s

8.3.2 Case 3 – 100 kg/s release of Methane

Figure 61 shows the volume fraction contour map of 100 kg/s release of methane from 25 cm hole in the modified geometry.

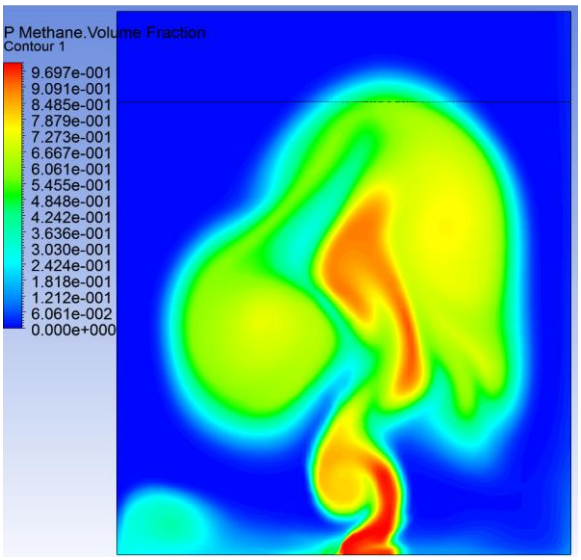

Figure 61: Volume fraction for 100 kg/s

8.3.3 Discussion

Figure 59, Figure 60 and Figure 61 represent the volume fraction contour map results from the release of methane at different flow rates. The width has no effect now on the dispersion of methane on both the water and air bodies. As the flow rate increases, the rise time decreases and the more methane escapes to the surface. The rise time, methane percentage on the surface, mass flux were reported in the following Table 32.

Table 32: Parameters estimated from expanded 50 m simulations

Flowrate kg/s	Simulation Rise Time (sec)	Methane Percentage on the surface %	Mass Flux ($kg/m^2.s$)
20	9	27	2.8
50	7	33	4.2
100	6	42	7.5

If the third case is to be considered as an offshore real case scenario. If methane was released at 100 kg/s from 25 cm release diameter, it will reach to the surface and disperse in the air body within 7 seconds. The percentage of the methane on the surface will be approximately 42 % with a mass flux of 7.5 $kg/m^2.s$ covering a big area of 500 m^2 (an area of 50 m width by 10 m height). According to the methane MSDS, the Lower Flammability Limit (LFL) and Upper Flammability Limit (UFL) of methane is 4.4% and 17 % respectively. The methane will not ignite in an area of 50 m width by 10 m high, however, the methane will keep dispensing and eventually it will ignite once methane percentage falls between LFL and UFL percentage ranges. The specified area of 50 m by 10 m will be considered as a toxic zone having very lethal concentrations of methane [56].

According to Olsen (2015), the aim of developing a general CFD model for shallow water is to simulate cases for high flow rate / high depth scenarios. It can be concluded that the extension of

this model covered part of the range of the concern suggested in Figure 62. The blue dots represent the three simulations presented in this section [2].

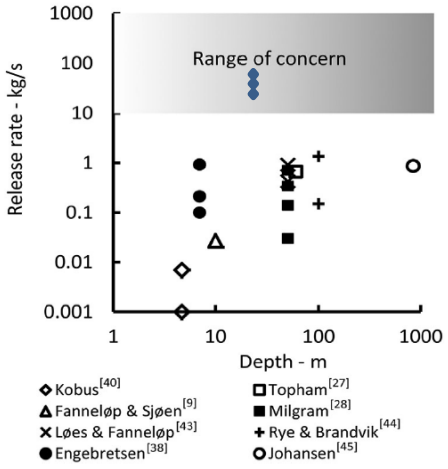

Figure 62: Depth/rate chart of subsea gas releases

8.3.4 H_2S Preliminary Study

In Qatar's offshore industry, natural gas is abundant and produced in large quantities. Qatar's natural gas is mainly methane with many impurities (e.g. H_2S, etc…). H_2S poses high risk by being a lethal toxic gas, slightly soluble in water and colorless gas. The Occupational Safety and Health Administration General Industry's Permissible Exposure Limit is a ceiling of 20 ppm with a 50 ppm 10-minute peak allowed once during an 8-hour shift. The National Institute for Occupational Safety and Health Immediately Dangerous to Life and Health concentration for H_2S is 100 ppm. In case of subsea gas releases incidents, usually, the gas released contains a percentage of H_2S. Thus a preliminary study was conducted to check the percentage of the H_2S dispersing on the surface in case of subsea gas release incident took place. The preliminary study will assume the following:

- Sour natural gas with 0.7 % of H_2S will be investigated,
- There will be no gas dissolution in the water body,
- The H_2S will follow the same behavior as the methane meaning that in case of 100 kg/s release 42 % of the H_2S will reach to the surface.

Table 33 represents the H_2S ppm levels on the surface knowing that 0.7 % of H_2S is released with methane. The preliminary study gives an insight into the worst case scenarios of H_2S levels expected on the surface.

Table 33: H_2S ppm dispersing on the surface

Flowrate kg/s	H_2S Percentage on the surface %	H_2S level
		ppm
20	0.19	1890
50	0.23	2310
100	0.29	2940

As indicated in

Table 33, the H2S ppm levels are very high ranging from 1890 ppm to almost 3000 ppm compared to Dangerous to Life and Health concentration of 100 ppm. The H_2S dispersion cannot be neglected in case of any subsea gas release as it will cause death to all workers in the offshore platform. In addition, the H_2S will keep dispersing in the air and might reach to other platforms. If the concentration is too high, it might affect the cities around the offshore platform area.

9 CONCLUSION AND FUTURE WORK

The main objective of this thesis is to improve a general CFD framework using the state of the art, previous CFD models and different configurations to model subsea gas release. First, the importance of modeling subsea gas releases was addressed from a process safety point of view followed by repeated incidents happened in the industry. These incidents raised the awareness to predict such phenomena as it will help in both incidents investigation and planning a proper emergency response. There are two types of models to simulate subsea release, the integral models, and the CFD models. In chapter two, different integral models were discussed and analyzed. The integral models showed lots of deficiencies in accounting of turbulence and predicting the dispersion/interactions on the surface zone. On the other side, recent studies on CFD tools showed fair performance but still there is a large area for improvements. First, a CFD model was developed using Eulerian – Eulerian approach and the RNG $k-\varepsilon$ model and tested against the Rotvoll experimental data by the various simulations preformed. The overall simulation results are found to yield very good agreement with the experimental data. The model was further expanded to model Arabian Gulf subsea gas release cases in Qatar. The conducted simulations also covered part of the range of concern (depth / rate) chart developed by Oil & Gas offshore companies. Finally. An H_2S preliminary release study concluded that the H_2S levels at the surface are significant and cannot be neglected in case of subsea gas releases risk assessment.

Further work on the model is necessary to improve the accuracy of the risk assessment for subsea gas releases, in case of incidents investigation. The future work should be as follows:

1- Cover bigger part of the range of concern (Figure 62) by SINTEF by simulating different scenarios at more release depths and rates.

2- Phenomena that need to be added and enabled in the model to further improve the setup.

- Sea current: it has a great effect on the gas released due to the relative low buoyancy of the gas. For example, recreating the ocean currents by defining new vertical water boundaries as velocity inlet or patch in pre-calculated velocity values in both x and y directions.
- H_2S: include different composition of H_2S, CO_2 and different NG's impurities.
- Gas dissolution: a study has to be carried out to check the effect of impurities included with methane on the dispersion of the released gas in the water body. The study should conclude whether the effect of gas dissolution should be included or not.
- Water stratification effect will be included in by defining different water properties (e.g. temperature, density, and salinity) at different locations based on the variation in depth.

REFERENCES

[1] T. Engebresten, T. Northug, K. Sjoen, and T. K. Fannelop, “Surface Flow and Gas Dispersion from a Subsea Release of Natural Gas,” in *Proceedings of the Seventh (1997) International Offshore and Polar Engineering Conference*, 1997, vol. I.

[2] J. E. Olsen and P. Skjetne, “Current understanding of subsea gas release: A review,” *Can. J. Chem. Eng.*, vol. 94, no. 2, pp. 209–219, 2016.

[3] J. E. Olsen and P. Skjetne, “GOVERNING PHYSICS OF SHALLOW AND DEEP SUBSEA GAS RELEASE,” in *10th International Conference on CFD in Oil & Gas, Metallurgical and Process Industries*, 2014.

[4] C. Daniel and J. F. Louvar, *Chemcial Process Safety: fundamantals with Applications (3rd Edition)*, 3rd Editio. 2011.

[5] C. Zoe and H. Kate, “Pipeline failure rates for land use planning assessments,” 2015.

[6] CCPS (Center for Chemical Process Safety), *Guidelines for Developing Quantitative Safety Risk Criteria*. 2009.

[7] T. Finn, “Barzan Field Incident,” *Reuters*, 2016. [Online]. Available: https://www.reuters.com/article/qatar-gas-barzan/corrected-update-1-gas-leak-delays-start-up-of-qatars-barzan-gas-project-sources-idUSL8N1CN2BY. [Accessed: 20-Nov-2017].

[8] M. J. Friedl and T. K. Fanneløp, “Bubble plumes and their interaction with the water surface,” *Appl. Ocean Res.*, vol. 22, no. 2, pp. 119–128, 2000.

[9] T. FANNELOP and K. SJOEN, “Hydrodynamics of Underwater Blowouts,” *18th Aerosp. Sci. Meet.*, 1980.

[10] M. S. G. Bettelini and T. K. Fanneløp, “Underwater plume from an instantaneously started

source," *Appl. Ocean Res.*, vol. 15, no. 4, pp. 195–206, 1993.

[11] S.L. Ross Environmental Research Ltd., "Fate and Behavior of Deepwater Subsea Oil Well Blowouts in the Gulf of Mexico," no. October, p. 25, 1997.

[12] K. E. Einarsrud and I. Brevik, "Kinetic Energy Approach to Dissolving Axisymmetric Multiphase Plumes," *J. Hydraul. Eng.*, vol. 135, no. 12, pp. 1041–1051, 2013.

[13] P. J. Rew, P. Gallagher, and D. M. Deaves, "Dispersion of Subsea Releases. Review of prediction methodologies," 1995.

[14] Innomar, "Shallow Water depth," *Innomar*, 2014. [Online]. Available: https://www.innomar.com/application-shallow-water.php. [Accessed: 16-Sep-2017].

[15] N. W. A. Encylopedia, "Depth of Arabian Gulf," *New World AgencyEncylopedia*, 2015. [Online]. Available: http://www.newworldencyclopedia.org/entry/Persian_Gulf. [Accessed: 10-Sep-2017].

[16] R. Darby, *Chemical Engineering Fluid Mechanics*. CRC, 2001.

[17] D. A. Engelbertha, "Experimental and modeling study of subsea releases of oil and gas," Norwegian University of Science and Technology, 2015.

[18] Ø. Johansen, *Deep water plume models - What's special about deep water Deep water blowouts - knowledge basis*. 2014.

[19] J. Ditmars and K. Cederwall, "ANALYSIS OF AIR-BUBBLE PLUMES," pp. 1257–1261, 1974.

[20] F. Energy, "Detection of Hydrates on Gas Bubbles during a Subsea Oil / Gas Leak," no. July, 2015.

[21] G. Janicki, S. Schlöter, T. Hennig, and G. Deerberg, "Simulation of subsea gas hydrate exploitation," *Energy Procedia*, vol. 59, pp. 82–89, 2014.

[22] Ø. Johansen, “DeepBlow – a Lagrangian Plume Model for Deep Water Blowouts,” *Spill Sci. Technol. Bull.*, vol. 6, no. 2, pp. 103–111, 2000.

[23] S. A. Socolofsky, E. E. Adams, and C. R. Sherwood, “Formation dynamics of subsurface hydrocarbon intrusions following the Deepwater Horizon blowout,” *Geophys. Res. Lett.*, vol. 38, no. 9, pp. 2–7, 2011.

[24] J. D. Ditmars and N. H. Brooks, “ANALYSIS OF AIR-BUBBLE PLUMES,” 1970.

[25] H. Kobus, “ANALYSIS OF THE FLOW INDUCED BY AIR-BUBBLE SYSTEMS,” pp. 1137–1147, 1970.

[26] J. H. Milgram, “Mean flow in round bubble plumes,” *J. Fluid Mech.*, vol. 133, pp. 345–376, 1983.

[27] J. H. Milgram and J. J. Burgess, “Measurements of the surface flow above round bubble plumes,” *Appl. Ocean Res.*, vol. 6, no. 1, pp. 40–44, 1984.

[28] P. D. Yapa, Z. Li, and L. Zheng, “Simulation of oil spills from underwater accidents I: Model development Simulation of oil spills from underwater accidents I: Model development Simulation de déversements de pétrole dus a accidents sous-marins I: Elaboration du modèle,” *J. Hydraul. Res.*, vol. 355, no. November, pp. 673–688, 1997.

[29] T. Moros and I. Dand, “Two-Phase Flows as a Result of a Subsea Blowout and Their,” no. 1, 1990.

[30] C. Swan and A. Moros, “The hydrodynamics of a subsea blowout,” *Appl. Ocean Res.*, vol. 15, no. 5, pp. 269–280, 1993.

[31] P. D. Yapa, L. K. Dasanayaka, U. C. Bandara, and K. Nakata, “A model to simulate the transport and fate of gas and hydrates released in deepwater,” *J. Hydraul. Res.*, vol. 48, no. 5, pp. 559–572, 2010.

[32] A. Workbench, “Ansys Fluent workbench userguide.” [Online]. Available: https://www.sharcnet.ca/Software/Ansys/16.2.3/en-us/help/flu_wb/flu_wb.html.

[33] D. D. Joseph, T. S. Lundgren, R. Jackson, and D. A. Saville, “Ensemble averaged and mixture theory equations for incompressible fluid-particle suspensions,” *Int. J. Multiph. Flow*, vol. 16, no. 1, pp. 35–42, 1990.

[34] L. Mazzei, “Eulerian modelling and computational fluid dynamics simulation of mono and polydisperse fluidized suspension,” no. October, p. 191, 2008.

[35] N. C. Markatos, “The mathematical modelling of turbulent flows,” *Appl. Math. Model.*, vol. 10, no. 3, pp. 190–220, 1986.

[36] W. Malalasekera and H. K. Versteeg, *An Introduction to Computational Fluid Dynamics - The Finite Volume Method*, vol. 44, no. 2. 2006.

[37] C. D. Argyropoulos and N. C. Markatos, “Recent advances on the numerical modelling of turbulent flows,” *Appl. Math. Model.*, vol. 39, no. 2, pp. 693–732, 2015.

[38] E. Furbo, “Evaluation of RANS turbulence models for flow problems with significant impact of boundary layers,” *Thesis*, no. December, p. 56, 2010.

[39] S. Cloete, J. E. Olsen, and P. Skjetne, “CFD modeling of plume and free surface behavior resulting from a sub-sea gas release,” *Appl. Ocean Res.*, vol. 31, no. 3, pp. 220–225, 2009.

[40] P. Skjetne and J. E. Olsen, “A Parcel Based Modeling Concept for studying subsea gas release and the effect of gas dissolution,” *Prog. Comput. Fluid Dyn.*, vol. 12, no. Nos.2/3, pp. 187–195, 2012.

[41] K. Wu, S. Cunningham, S. Sivandran, and J. Green, “Modelling subsea gas releases and resulting gas plumes using Computational Fluid Dynamics,” *J. Loss Prev. Process Ind.*, vol. 49, pp. 411–417, 2017.

[42] B. E. Launder and B. I. Sharma, “Application of the energy-dissipation model of turbulence to the calculation of flow near a spinning disc,” *Lett. Heat Mass Transf.*, vol. 1, no. 2, pp. 131–137, 1974.

[43] D. C. Wilcox, *Turbulence modeling for CFD*, 3rd ed. La Cãnada, Calif. : DCW Industries, [2006], 2006.

[44] V. Yakhot and S. A. Orszag, “Renormalization group analysis of turbulence. I. Basic theory,” *J. Sci. Comput.*, vol. 1, no. 1, pp. 3–51, 1986.

[45] V. Yakhot, S. A. Orszag, S. Thangam, T. B. Gatski, and C. G. Speziale, “Development of turbulence models for shear flows by a double expansion technique,” *Phys. Fluids A*, vol. 4, no. 7, pp. 1510–1520, 1992.

[46] B. R. Morton, G. Taylor, and J. S. Turner, “Turbulent Gravitational Convection from Maintained and Instantaneous Sources,” *Proc. R. Soc. A Math. Phys. Eng. Sci.*, vol. 234, no. 1196, pp. 1–23, 1956.

[47] L. Billeter and T. K. Fanneløp, “Gas concentration over an underwater gas release,” *Atmos. Environ.*, vol. 23, no. 8, pp. 1683–1694, 1989.

[48] J. E. Olsen and P. Skjetne, “Modelling of underwater bubble plumes and gas dissolution with an Eulerian-Lagrangian CFD model,” *Appl. Ocean Res.*, vol. 59, pp. 193–200, 2016.

[49] M. C. Kara, M. Parsi, P. P. Sharma, and A. Jatale, “CFD MODELING OF SUBSEA GAS RELEASES USING AN IMPROVED BUBBLE DRAG LAW,” pp. 1–7, 2017.

[50] A. Sayma, “Computational Fluid Dynamics.” 2009.

[51] R. B. Bird, W. Stewart, and E. Lightfoot, *Transport Phenomena*. 2002.

[52] A. De Souza, *How to – Understand Computational Fluid Dynamics Jargon*. 2005.

[53] A. Bakker, “Lecture 6 - Boundary Conditions Applied Computational Fluid Dynamics,”

Fluid Dyn., no. 2002, pp. 1–31, 2006.

[54] P. Vollestad, “Modeling of Subsea gas releases,” NTNU, Trondheim, Norway, 2014.

[55] Sharcnet, “Turbulence models,” 2016. [Online]. Available: https://www.sharcnet.ca/Software/Ansys/16.2.3/en-us/help/flu_th/flu_th_sec_turb_rng.html.

[56] E. Overview, “Praxair Material Safety Data Sheet,” no. February, pp. 2004–2005, 2005.

[57] R. Bhaskaran and L. Collins, “Introduction to CFD basics,” 2015.

APPENDIX A: CFD GOVERNING EQUATIONS

Most of the CFD applications are developed based on the fundamentals of governing equation of fluid dynamics which are the conservation of mass, momentum, and energy.[51]. In ANSYS Fluent, the software solves the conservation equation of mass and momentum. However, for the energy equation, it requires the enabling of the heat transfer or compressibility to be included in the solving process [32].

Conservation of mass

According to the Transport Phenomena book by Bird et al. [51], the conservation of mass or the continuity equation can be represented for both incompressible and compressible flow as follows,

$$\frac{\partial \rho}{\partial t} + \nabla . (\rho \vec{v}) = 0 \qquad \text{Equation 39}$$

Where ρ is the density and $\vec{v}$ is the velocity vector for three dimensions which is represented by

$$\overrightarrow{V_i} = u_i \, \hat{\imath} + v_i \, \hat{\jmath} + \mathrm{w_i} \, \hat{k} \qquad \text{Equation 40}$$

The operator ∇ will be in the form of

$$\nabla = \hat{\imath} \frac{\partial}{\partial x} + \hat{\jmath} \frac{\partial}{\partial y} + \hat{k} \frac{\partial}{\partial z} . \qquad \text{Equation 41}$$

Conservation of momentum

The conservation of momentum is defined in ANSYS Fluent as follows [51]:

$$\frac{\partial}{\partial t}(\rho\vec{v}) + \nabla . (\rho\vec{v}\vec{v}) = -\nabla p + \nabla . (\bar{\bar{\tau}}) + \rho\vec{g} \quad \text{Equation 42}$$

Where p is the static pressure, g is the gravitational body force and $\bar{\bar{\tau}}$ is the stress tensor given by the following equation [36],

$$\bar{\bar{\tau}} = \mu \left[(\nabla\vec{v} + \nabla\vec{v}^{T}) - \frac{2}{3}\nabla . \vec{v} I \right] \quad \text{Equation 43}$$

Where I is the unit tensor and μ is the molecular viscosity.

For the incompressible flow, the momentum equations can be represented as follows for the Cartesian coordinates [51],

$$\rho\left(\frac{\partial v_x}{\partial t} + v_x\frac{\partial v_x}{\partial x} + v_y\frac{\partial v_x}{\partial y} + v_z\frac{\partial v_x}{\partial z}\right) = \frac{\partial p}{\partial x} - \left[\frac{\partial^2 v_x}{\partial x^2} + \frac{\partial^2 v_x}{\partial y^2} + \frac{\partial^2 v_x}{\partial z^2}\right] + \rho g_x \quad \text{Equation 44}$$

$$\rho\left(\frac{\partial v_y}{\partial t} + v_x\frac{\partial v_y}{\partial x} + v_y\frac{\partial v_y}{\partial y} + v_z\frac{\partial v_y}{\partial z}\right) = \frac{\partial p}{\partial y} - \left[\frac{\partial^2 v_y}{\partial x^2} + \frac{\partial^2 v_y}{\partial y^2} + \frac{\partial^2 v_y}{\partial z^2}\right] + \rho g_y \quad \text{Equation 45}$$

$$\rho\left(\frac{\partial v_z}{\partial t} + v_x\frac{\partial v_z}{\partial x} + v_y\frac{\partial v_z}{\partial y} + v_z\frac{\partial v_z}{\partial z}\right) = \frac{\partial p}{\partial z} - \left[\frac{\partial^2 v_z}{\partial x^2} + \frac{\partial^2 v_z}{\partial y^2} + \frac{\partial^2 v_z}{\partial z^2}\right] + \rho g_z \quad \text{Equation 46}$$

Some books [36], [50], [57] add an extra term to the abovementioned equation which is the source term S_i to account for external forces ex, (drag force and heat source).

APPENDIX B: 50 METERS CONTOUR MAPS

20 kg/s release of methane

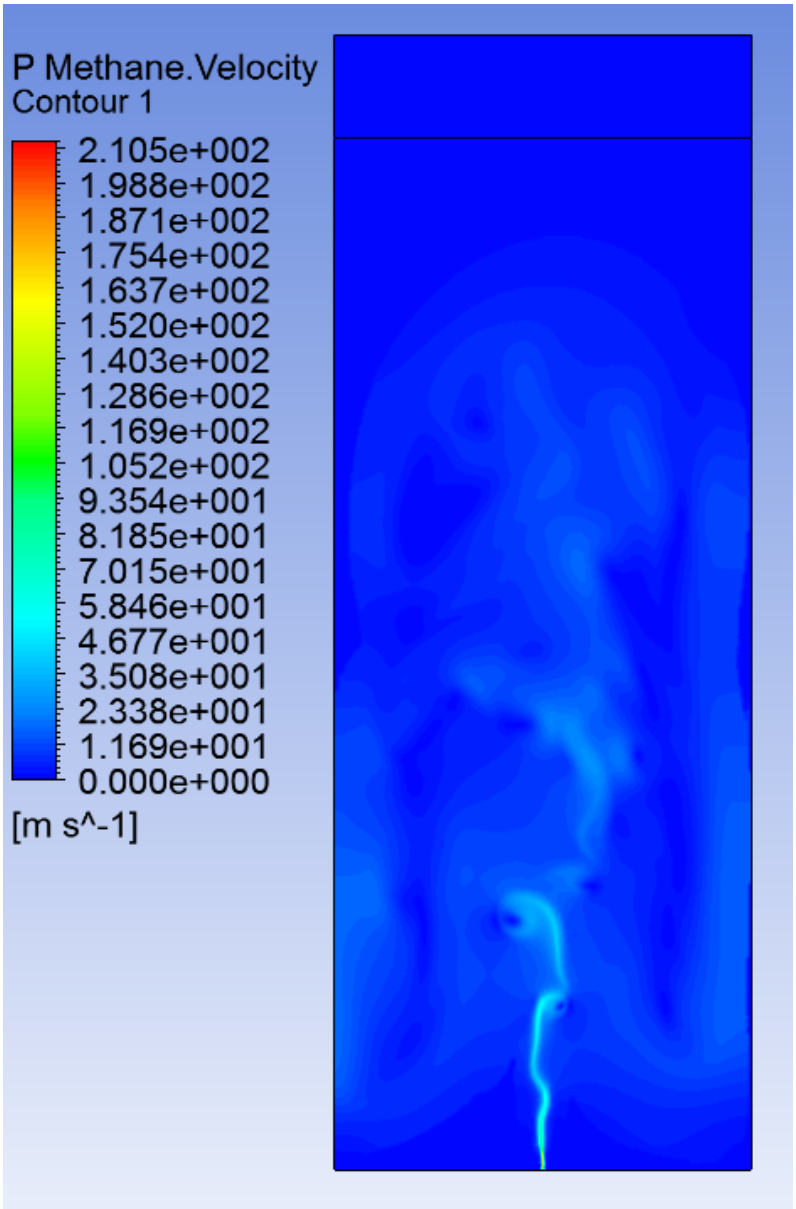

Figure 63: Velocity contour map

50 kg/s release of methane

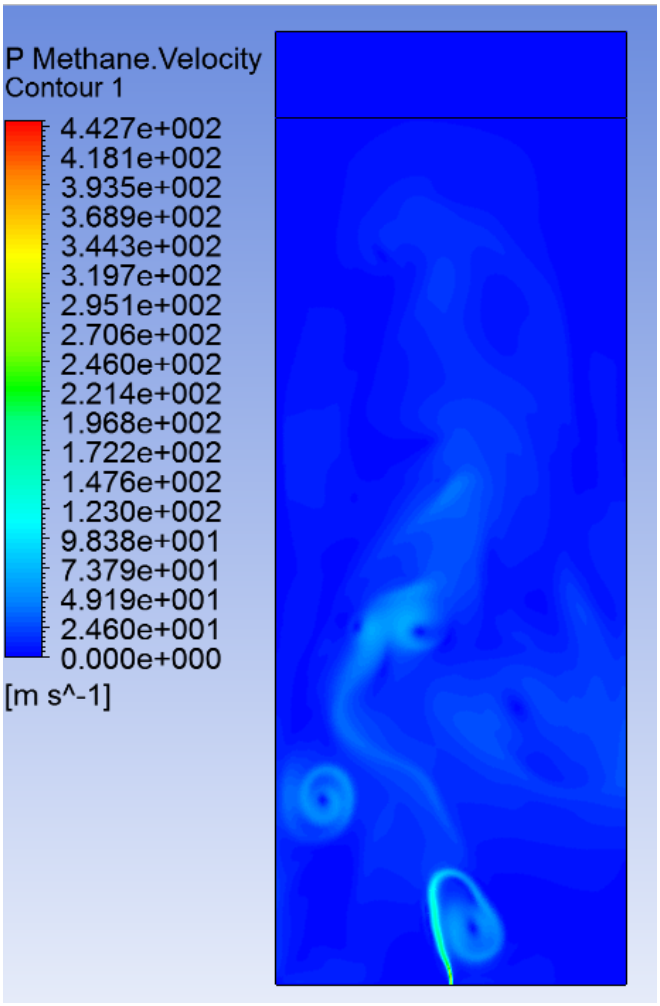

Figure 64: Velocity contour map

100 kg/s release of methane

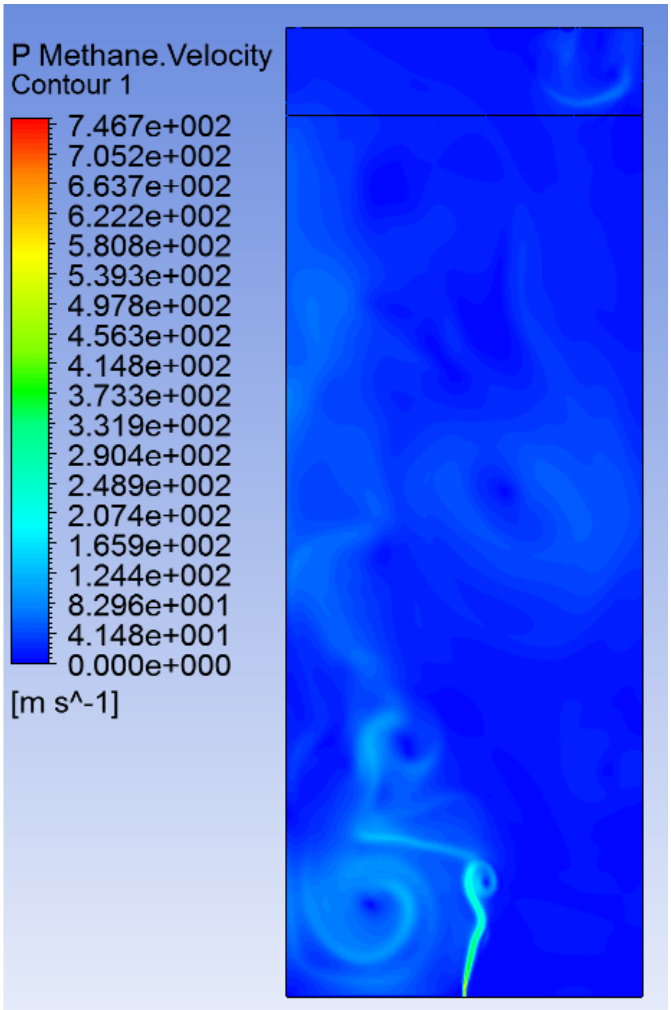

Figure 65: Velocity contour map